



**Defense Nuclear Agency  
Alexandria, VA 22310-3398**



**DNA-TR-95-106**

## **Innovative Pulsed Power Diagnostics for Radiation Simulators**

**Nino R. Pereira  
Berkeley Research Associates, Inc  
P.O. Box 241  
Berkeley, CA 94701-0241**

**June 1996**

**DATA QUALITY ASSURED**

**Technical Report**

**CONTRACT No. DNA 001-94-C-0196**

Approved for public release;  
distribution is unlimited.

**19960610 175**

Destroy this report when it is no longer needed. Do not return to sender.

PLEASE NOTIFY THE DEFENSE NUCLEAR AGENCY,  
ATTN: CSTI, 6801 TELEGRAPH ROAD, ALEXANDRIA, VA  
22310-3398, IF YOUR ADDRESS IS INCORRECT, IF YOU  
WISH IT DELETED FROM THE DISTRIBUTION LIST, OR  
IF THE ADDRESSEE IS NO LONGER EMPLOYED BY YOUR  
ORGANIZATION.



## DISTRIBUTION LIST UPDATE

This mailer is provided to enable DNA to maintain current distribution lists for reports. (We would appreciate your providing the requested information.)

- ☐ Add the individual listed to your distribution list.
- ☐ Delete the cited organization/individual.
- ☐ Change of address.

### NOTE:

Please return the mailing label from the document so that any additions, changes, corrections or deletions can be made easily. For distribution cancellation or more information call DNA/IMAS (703) 325-1036.

NAME: \_\_\_\_\_

ORGANIZATION: \_\_\_\_\_

### OLD ADDRESS

### CURRENT ADDRESS

\_\_\_\_\_  
\_\_\_\_\_  
\_\_\_\_\_

\_\_\_\_\_  
\_\_\_\_\_  
\_\_\_\_\_

TELEPHONE NUMBER: (    ) \_\_\_\_\_

### DNA PUBLICATION NUMBER/TITLE

### CHANGES/DELETIONS/ADDITIONS, etc.) (Attach Sheet if more Space is Required)

\_\_\_\_\_  
\_\_\_\_\_  
\_\_\_\_\_

\_\_\_\_\_  
\_\_\_\_\_  
\_\_\_\_\_

DNA OR OTHER GOVERNMENT CONTRACT NUMBER: \_\_\_\_\_

CERTIFICATION OF NEED-TO-KNOW BY GOVERNMENT SPONSOR (if other than DNA): \_\_\_\_\_

SPONSORING ORGANIZATION: \_\_\_\_\_

CONTRACTING OFFICER OR REPRESENTATIVE: \_\_\_\_\_

SIGNATURE: \_\_\_\_\_

CUT HERE AND RETURN



DEFENSE NUCLEAR AGENCY  
ATTN: IMAS  
6801 TELEGRAPH ROAD  
ALEXANDRIA, VA 22310-3398

DEFENSE NUCLEAR AGENCY  
ATTN: IMAS  
6801 TELEGRAPH ROAD  
ALEXANDRIA, VA 22310-3398

| REPORT DOCUMENTATION PAGE  |   |   | Form Approved<br>OMB No. 0704-0188    |  |
|--|---|---|---------------------------------------|--|
| Public reporting burden for this collection of information is estimated to average 1 hour per response including the time for reviewing instructions, searching existing data sources, gathering and maintaining the data needed, and completing and reviewing the collection of information. Send comments regarding this burden estimate or any other aspect of this collection of information, including suggestions for reducing this burden, to Washington Headquarters Services Directorate for information Operations and Reports, 1215 Jefferson Davis Highway, Suite 1204, Arlington, VA 22202-4302, and to the Office of Management and Budget, Paperwork Reduction Project (0704-0188), Washington, DC 20503.   |   |   |                                       |  |
| 1. AGENCY USE ONLY (Leave blank)   | 2. REPORT DATE<br>960601                                    | 3. REPORT TYPE AND DATES COVERED<br>Technical 940930 - 950929   |                                       |  |
| 4. TITLE AND SUBTITLE<br><br>Innovative Pulsed Power Diagnostics for Radiation Simulators  |   | 5. FUNDING NUMBERS<br>C - DNA 001-94-C-0196<br>PE - 62715H<br>PR - G<br>TA - E<br>WU - DH800790<br>DH345860 |                                       |  |
| 6. AUTHOR(S)<br><br>Nino R. Pereira  |   |   |                                       |  |
| 7. PERFORMING ORGANIZATION NAME(S) AND ADDRESS(ES)<br>Berkeley Research Associates, Inc.<br>P.O. Box 241<br>Berkeley, CA 94701-0241  |   | 8. PERFORMING ORGANIZATION<br>REPORT NUMBER<br><br>BRA-96-W017R   |                                       |  |
| 9. SPONSORING/MONITORING AGENCY NAME(S) AND ADDRESS(ES)<br>Defense Nuclear Agency<br>6801 Telegraph Road<br>Alexandria, VA 22310-3398<br>EST/Schneider   |   | 10. SPONSORING/MONITORING<br>AGENCY REPORT NUMBER<br><br>DNA-TR-95-106                                      |                                       |  |
| 11. SUPPLEMENTARY NOTES<br>This work was sponsored by the Defense Nuclear Agency under RDT&E RMC Code B4662D G E 00035 3300A 25904D.   |   |   |                                       |  |
| 12a. DISTRIBUTION/AVAILABILITY STATEMENT<br><br>Approved for public release; distribution is unlimited.  |   |   | 12b. DISTRIBUTION CODE                |  |
| 13. ABSTRACT (Maximum 200 words)<br>This report describes the accomplishments during the first year of Contract DNA 001-94-C-0196. The various x-ray spectrometers progress quite well. Our subcontractor, Physics International Company, has successfully tested the time-resolved soft x-ray crystal spectrometer, using a borrowed streak camera. This instrument will be purchased, configured in the appropriate way, and used for PRS tests next year. Likewise, the spatially resolved hard x-ray spectrometer is progressing very well. Time-integrated tests agree with expectations. A prototype scintillator-fiberoptic dose rate monitor for this instrument has been built, and works well. Further tests are planned on DM1 in the near future.<br><br>The current diagnostic for high linear current, the responsibility of our subcontractor MRC, can be a carefully designed B-dot probe. The originally proposed diagnostic, based on measuring the shock from magnetic pressure, will receive less emphasis. The voltage meter using ion range filtering is waiting for a scintillator-fiberoptic dose rate monitor and an optical streak camera. A simple debris diagnostic has shown that debris from an aluminum pinch on Phoenix penetrates only about 3 mg/cm <sup>2</sup> of material irrespective of size. |   |   |                                       |  |
| 14. SUBJECT TERMS<br>Ion Range Voltage Meter<br>High Linear Current Diagnostic<br>Time-Resolved X-Ray Spectrometer   |   |   | 15. NUMBER OF PAGES<br>44             |  |
| Soft X-Rays<br>Bremsstrahlung<br>Debris Diagnostic   |   |   | 16. PRICE CODE                        |  |
| 17. SECURITY CLASSIFICATION<br>OF REPORT<br>UNCLASSIFIED   | 18. SECURITY CLASSIFICATION<br>OF THIS PAGE<br>UNCLASSIFIED | 19. SECURITY CLASSIFICATION<br>OF ABSTRACT<br>UNCLASSIFIED  | 20. LIMITATION OF ABSTRACT<br><br>SAR |  |

UNCLASSIFIED

SECURITY CLASSIFICATION OF THIS PAGE

CLASSIFIED BY:

N/A since Unclassified.

DECLASSIFY ON:

N/A since Unclassified.

## SUMMARY

This report describes the accomplishments during the first year of Contract DNA001-94-C-0196. The various x-ray spectrometers progress quite well. Our subcontractor Physics International has successfully tested the time-resolved soft x-ray crystal spectrometer, using a borrowed streak camera. This instrument will be purchased, configured in the appropriate way, and used for PRS tests next year.

Likewise, the spatially resolved hard x-ray spectrometer is progressing very well. Time-integrated tests agree with expectations. A prototype scintillator-fiberoptic dose rate monitor for this instrument has been built, and works well. Further tests are planned on DM1 in the near future.

The current diagnostic for high linear current, the responsibility of our subcontractor MRC, can be a carefully designed B-dot. The originally proposed diagnostic, based on measuring the shock from magnetic pressure, will receive less emphasis. The voltage meter using ion range filtering is waiting for the a scintillator-fiberoptic dose rate monitor and an optical streak camera. A simple debris diagnostic has shown that debris from an aluminum pinch on Phoenix penetrates only about  $3 \text{ mg/cm}^2$  of material, irrespective of debris size.

# CONVERSION TABLE

Conversion factors for U.S. Customary to metric (SI) units of measurement

MULTIPLY —————> BY —————> TO GET  
TO GET< ————— BY < ————— DIVIDE

|  |                                   |         |  |
|--|-----------------------------------|---------|--|
| angstrom   | 1.000 000                         | X E -10 | meters (m)                                     |
| atmosphere (normal)                              | 1.013 25 X E +2                   |         | kilo pascal (kPa)                              |
| bar  | 1.000 000                         | X E +2  | kilo pascal (kPa)                              |
| barn   | 1.000 000                         | X E -28 | meter <sup>2</sup> (m <sup>2</sup> )           |
| British thermal unit (thermochemical)            | 1.054 350                         | X E +3  | joule (J)                                      |
| calorie (thermochemical)                         | 4.184 000                         |         | joule (J)                                      |
| cal (thermochemical)/cm <sup>2</sup>             | 4.184 000                         | X E -2  | mega joule/m <sup>2</sup> (MJ/m <sup>2</sup> ) |
| curie  | 3.700 000                         | X E +1  | *giga becquerel (GBq)                          |
| degree (angle)                                   | 1.745 329                         | X E -2  | radian (rad)                                   |
| degree Fahrenheit                                | $T_K = (T^{\circ}F + 459.67)/1.8$ |         | degree kelvin (K)                              |
| electron volt                                    | 1.602 19 X E -19                  |         | joule (J)                                      |
| erg  | 1.000 000                         | X E -7  | joule (J)                                      |
| erg/second                                       | 1.000 000                         | X E -7  | watt (W)                                       |
| foot   | 3.048 000                         | X E -1  | meter (m)                                      |
| foot-pound-force                                 | 1.355 818                         |         | joule (J)                                      |
| gallon (U.S. liquid)                             | 3.785 412                         | X E -3  | meter <sup>3</sup> (m <sup>3</sup> )           |
| inch   | 2.540 000                         | X E -2  | meter (m)                                      |
| jerk   | 1.000 000                         | X E +9  | joule (J)                                      |
| joule/kilogram (J/kg) (radiation dose absorbed)  | 1.000 000                         |         | Gray (Gy)                                      |
| kilotons   | 4.183                             |         | terajoules                                     |
| kip (1000 lbf)                                   | 4.448 222                         | X E +3  | newton (N)                                     |
| kip/inch <sup>2</sup> (ksi)                      | 6.894 757                         | X E +3  | kilo pascal (kPa)                              |
| ktap   | 1.000 000                         | X E +2  | newton-second/m <sup>2</sup> —                 |
| micron   | 1.000 000                         | X E -6  | (N-s/m <sup>2</sup> )                          |
| mil  | 2.540 000                         | X E -5  | meter (m)                                      |
| mile (international)                             | 1.609 344                         | X E +3  | meter (m)                                      |
| ounce  | 2.834 952                         | X E -2  | meter (m)                                      |
| pound-force (lbs avoirdupois)                    | 4.448 222                         |         | kilogram (kg)                                  |
| pound-force inch                                 | 1.129 848                         | X E -1  | newton (N)                                     |
| pound-force/inch                                 | 1.751 268                         | X E +2  | newton/meter (N · m)                           |
| pound-force/foot <sup>2</sup>                    | 4.788 026                         | X E -2  | newton-meter (N/m)                             |
| pound-force/inch <sup>2</sup> (psi)              | 6.894 757                         |         | kilo pascal (kPa)                              |
| pound-mass (lbm avoirdupois)                     | 4.535 924                         | X E -1  | kilo pascal (kPa)                              |
| pound-mass-foot <sup>2</sup> (moment of inertia) | 4.214 011                         | X E -2  | kilogram (kg)                                  |
| pound-mass-foot <sup>3</sup>                     | 1.601 846                         | X E +1  | kilogram-meter <sup>2</sup>                    |
| rad (radiation dose absorbed)                    | 1.000 000                         | X E -2  | (kg-m <sup>2</sup> )                           |
| roentgen   | 2.579 760                         | X E -4  | kilogram/meter <sup>3</sup>                    |
| shake  | 1.000 000                         | X E -8  | (kg/m <sup>3</sup> )                           |
| slug   | 1.459 390                         | X E +1  | **Gray (Gy)                                    |
| torr (mm Hg, 0°C)                                | 1.333 22 X E -1                   |         | coulomb/kilogram                               |
|  |                                   |         | (C/kg)   |
|  |                                   |         | second (s)                                     |
|  |                                   |         | kilogram (kg)                                  |
|  |                                   |         | kilo pascal (kPa)                              |

\* The Becquerel (Bq) is the SI unit of radioactivity; 1 Bq = 1 event/s.

\*\* The Gray (GY) is the SI unit of absorbed radiation.

## TABLE OF CONTENTS

| Section                            | Page |
|------------------------------------|------|
| SUMMARY                            | iii  |
| CONVERSION TABLE                   | iv   |
| FIGURES                            | vi   |
| 1 HARD BREMSSTRAHLUNG SPECTROMETER | 1    |
| 2 SOFT X-RAY SPECTROMETER          | 12   |
| 3 VOLTMETER                        | 16   |
| 4 DEBRIS                           | 20   |
| 5 CURRENT PROBE                    | 23   |
| Appendix                           |      |
| X-RAY STREAK CAMERA                | A-1  |

## FIGURES

| Figure  | Page |
|---|------|
| 1-1 Design of the spectrometer.   | 5    |
| 1-2 Response functions for the time-integrated spectrometer with $\text{CaF}_2$ .   | 6    |
| 1-3 Response functions for the time-resolved spectrometer<br>with plastic scintillator.   | 7    |
| 1-4 Comparison between measurements and expectations<br>for the Compton-Hall section.   | 8    |
| 1-5 Comparison between measurements and expectations<br>for the absorber section.   | 9    |
| 1-6 Designs of the optical scintillator-fiber dose rate monitor.  | 10   |
| 1-7 Signal produced by the optical dose rate monitor<br>intended for the absorber stack.  | 11   |
| 3-1 Construction of the filter stack for the voltmeter.   | 19   |
| 5-1 Current profile with linear and nonlinear penetration at 40 ns and 80 ns.   | 26   |
| 5-2 Signal from a PVDF sensor with a laser-driven shock.  | 27   |
| A-1 Geometry of streak camera setup on Double Eagle.  | A-4  |
| A-2 Streaked spectrum for argon pinch.  | A-5  |
| A-3 Densitometer scan of lines at peak emission.  | A-6  |
| A-4 Spectrally integrated intensity from photodiode (PCD8)<br>compared to streaked $\text{Ar}_{He-\alpha}$ line (DE shot 3391). | A-7  |

## SECTION 1

### HARD BREMSSTRAHLUNG SPECTROMETER

Of all the different diagnostics that are to be developed under the present contract, the time resolved and spatially resolved hard bremsstrahlung spectrometer has received the most emphasis. This is because it is intended to be one of the main user diagnostics on DNA's future DECADE bremsstrahlung simulator. The instrument is patterned after an earlier time-resolved spectrometer that uses the same principle, namely differential filtering. However, the existing instrument is intended for isotropic radiation as might be seen by a user from a typical large area bremsstrahlung source. It is now located at DNA's Phoenix facility at NSWC, but available for use on DNA machines elsewhere. In fact, it will be used on the DECADE module DM1 starting the middle of November 1995.

The spatial resolution desired for the spectrometer has been the subject of some debate. The problem comes in because both the bremsstrahlung source and the test object are typically much larger than the distance in between the source and the test object. Both source and test object merit spatial resolution. However, on each point of a test object the radiation comes in isotropically, from the entire surface of the bremsstrahlung source. The existing spectrometer is appropriate for this case, except that its size is too large. The spectrometer's face is 10 cm  $\times$  10 cm, while the desired spatial resolution is 1 cm. In any case, the spectrometer would shadow the test object exactly at the measurement position, which is presumably the location where you want to test. For reasons like these we selected the other option, an instrument with 1 cm spatial resolution on the diode. This approach, and the accompanying conceptual design, was approved at the program at the beginning of the work.

The isotropic spectrometer's size can be shrunk substantially, to 4 cm square or so, by putting the spherical filters inside each other. It is also conceivable that dose enhancement at a high-Z/low-Z interface could be made into a much smaller energy-resolving sensor for a spectrometer. However, these possibilities were not available yet at the program review where the spatially resolved spectrometer's design was approved.

Figure 1-1 shows the hardware of the spatially resolved spectrometer. The x-rays come in from the right. Spatial resolution is obtained with a collimator, two 4 inch (10 cm) wide and 2 inch (5 cm) thick tungsten blocks with a 1 cm diameter hole through the center. At the end of the collimator is an aluminum Compton target. Behind the Compton target, in the Compton-Hall section, two 2-inch square magnets produce a magnetic field of 0.3 T over a 1 inch square opening. The difference between the responses on opposite sides gives energy resolution in the 0.5 MeV to 2 MeV photon energy range.

The Compton-Hall cavity has two linear arrays of detectors, one on each side of the aperture just downstream from the Compton target. Without the magnetic field there is a relatively uniform exposure across both arrays due to x-ray background, Compton-scattered x-rays, and the Compton electron spray. The magnetic field steers the Compton electrons toward detectors on one side, and away from detectors on the other side, but the background remains the same. The Compton electron contribution is isolated by subtracting the two sides.

Behind the Compton-Hall section is a conventional absorber stack with 8 stages to provide energy resolution between about 50 keV and 600 keV. The choice and thickness of the filters are taken from the previous instrument using spherical absorbers. They are thick enough that dose enhancement does not occur in the transition between two subsequent filters.

For time-integrated measurements the detectors can be ThermoLuminescent Detectors (TLDs), but for the final instrument these TLDs are replaced by scintillators coupled to fibers going into photomultipliers, or, if the signal levels permit, directly into an optical streak camera. For this DNA's streak cameras equipped with typical image intensifiers should work.

Unfolding the spectrum from the data is done with the code YOGI, in a standard way. Before YOGI can start it needs the responses of the different detectors as function of photon energy  $h\nu$ . These response functions  $R(h\nu)$  are computed using the ACCEPT member of the ITS suite of codes. The computation is done with the full geometry, accurate detector and filter materials, and for the Compton-Hall section the inclusion of an external magnetic field.

Figure 1-2 shows the response functions as computed for a time-integrated version of the instrument. Here the detectors are  $\text{CaF}_2$  TLDs. The left-most 8 response functions starting at about 20 keV up to 300 keV are for the  $\text{CaF}_2$  TLDs in the absorber stack. The tungsten filters, or absorbers, in between the TLDs increase their thickness in such a way that the response functions have equally spaced cutoffs on a logarithmic photon energy grid.

The filters must be so thick that electrons from a previous filter do not reach the subsequent stage. If this were not the case the filter/scintillator combinations would depend on their order in the stack. In the same vein, the magnetic field in the Compton-Hall section prevents electrons from the Compton target to get into the first filter. This lack of electrons might affect the dose in the first scintillator unless the first filter is thick enough to reach radiation equilibrium.

The right-most 5 response functions are for the differences between 5  $\text{CaF}_2$  TLDs on opposite sides in the Compton-Hall section. The energy cutoff is determined by the distance between TLD and Compton target, with the highest energy cutoff for the farthest TLD. The Compton-Hall responses are about an order of magnitude lower than those in the absorber section. The response is lower in part because it is the difference between two larger responses of sensors on opposite sides, but mostly because the Compton electrons are emitted in a widely dispersed spray. Only a fraction of these electrons is captured by the detector, which covers only a small part of the wall.

Figure 1-3 shows the response functions of the time-resolved version, exactly the same geometry but with the  $\text{CaF}_2$  TLDs replaced by plastic scintillators. The response functions' general features are the same, except for the much higher response of the TLDs than the scintillators at photon energies below about 100 keV. The reason is that the scintillator does not absorb the lower energy photons as strongly as the  $\text{CaF}_2$ , which has a higher average atomic number.

Figure 1-4 compares the dose measured in a far-field exposure on ARL's  $\text{Co}^{60}$  source with the dose expected from the known  $\text{Co}^{60}$  spectrum and the computed response

functions for the Compton-Hall section. The agreement is excellent, except perhaps for the lower-numbered TLDs closest to the Compton target. In the initial stages of the work we expected any problems to come up in the Compton-Hall section. This part is new and untried, and its response functions are much more complicated to compute due to the magnetic field. Moreover, the signals are lower. The good agreement is therefore particularly gratifying.

Figure 1-5 compares the dose measured in an exposure on ARL's  $\text{Co}^{60}$  source with the dose expected from the known  $\text{Co}^{60}$  spectrum and the computed response functions for the absorber section. It surprised us that the agreement is not as good as expected. The filter stack is a standard way of doing things, and we are confident in our ability to compute the response functions and the actual responses correctly.

At this time a possible reason for the discrepancy seems to be a measurement error. The instrument may not have been pointed correctly at the  $\text{Co}^{60}$  source, in which case part of the source is excluded. We are presently tracking this down by redoing these measurements. The good part here is that the collimator has proven its worth if a pointing error is indeed the cause of the discrepancy. Pointing errors can be avoided by a sight, which will be added to the design in the future.

The collimator has also been tested directly, by putting the instrument at the minimum distance (10 inches) from the  $\text{Co}^{60}$  source. The dose on the face of the aperture is  $80\times$  larger than at the position of the Compton target, and  $200\times$  larger than at the first detector position in the absorber stack, roughly as expected from a  $1/r^2$  falloff and the geometry.

What are the dose rates that the optical dose rate detector should be designed for? On DECADE the expected dose rate at 1 m is about  $4 \times 10^{10}$  rad/s. After collimation the expected dose rate on the first detector is then approximately  $2 \times 10^8$  rad/s. The detectors farther down in the stack, and those in the Compton-Hall section, may see an order of magnitude less radiation. The required range of the dose rate detectors must therefore exceed about  $10^7$  rad/s. Signals around 500 mV into a  $50\Omega$  cable require a current pulse from the dose rate detector around 10 mA, and the resulting sensitivity required of the dose rate detectors is from  $10^{-9}$  A/(rad/s) to  $5 \times 10^{-11}$  A/(rad/s).

For the time-resolved spectrometer we opted for an all-optical dose rate diagnostic. Figure 1-6 shows the two designs, the top one for the absorber stack and the bottom one for the Compton-Hall section. In the absorber stack, the scintillator must cover the entire opening of the collimator. Therefore the scintillator is a 3 mm thin plate with  $1 \text{ cm}^2$  area. In the Compton-Hall section the scintillator has the same area as the TLD. It is also 3 mm thick, the same mass per unit area of the TLD. The scintillator is a Bicron-Harshaw BC418 plastic, with a  $1/e$  decay constant specified as 0.5 ns.

Fibers are butted up to the scintillator from two perpendicular directions. The number of fibers can be increased if more light is needed. For our purposes there is ample light, and two to four fibers suffice. The fibers are protected from direct irradiation because they are in the shadow of the collimator.

The fibers are nominally 200  $\mu\text{m}$  core, high OH fused silica, step index doped, silica clad, with numerical aperture  $\lesssim 0.22$ . This type of fiber is widely available, and it is easy to work with, but it is not single mode. Temporal dispersion is not a problem, because for DECADE needs a fiber length of only 15 m. Multi-moding in the fiber then adds at most

1 ns to the time response of the system.

Light from the fibers comes into the photomultiplier through an array of filters. Narrow-band filters of 10 to 40 nm FWHM, centered around the peak of the scintillator output at 395 ns, help to exclude any Cherenkov background from the fibers. Moreover, narrow-band filtering of the scintillator light gives an effective decrease in the scintillator's time response.

The photomultiplier is a Hamamatsu type 1635P. The tube has a  $1 \text{ cm}^2$  photocathode, a nominal current gain of  $1 \times 10^6$ , and an FWHM impulse response time specified as 1.2 ns. In the standard bias configuration these photomultipliers are linear (to  $\pm 1\%$ ) provided the photocathode current density stays below  $1 \text{ nA/mm}^2$  and the anode current below 10 mA, corresponding to 0.5 V into a  $50\Omega$  cable.

The photomultiplier's time response can be improved somewhat by illuminating only a small fraction (perhaps 1/5) of the active photocathode area. Optimization of the time response of the entire scintillator-fiber-photomultiplier chain is presently underway. The expected overall pulse response time is 1.5 ns.

We prefer to operate all the photomultipliers from the same bias voltage, and to get comparable signals below 0.5 V on all the outputs. However, the expected amount of light from the scintillators differs by at least two orders of magnitude. Neutral density filters in between the fibers and the photomultipliers are intended to bring all the light back to a suitable level.

The bremsstrahlung source used for testing the optical dose rate monitors is stray radiation from ongoing shots on Aurora in the ion beam mode. Figure 1-7 shows the signal from a prototype of the scintillator-fiber design intended for the filter stack. To avoid overdriving the photomultiplier these tests have an ND-3 filter ( $1000\times$  attenuation) in addition to the narrow-band filter. The peak of the signal is 2.4 mA, or 120 mV, for a total charge of about 120 pC. The total dose on this shot as measured next to the scintillator is 20 rads. Therefore the sensitivity of the optical dose rate monitor is 6 pC/rad, or 6 pA/(rad/s). By taking away one or more of the neutral density filters the sensitivity in the present setup can be increased by three orders of magnitude.

As a result, the sensitivity to be expected from the optical dose rate monitor is about  $6 \times 10^{-9} \text{ A/(rad/s)}$ , and anything lower is obtainable by inserting filters. The dose rate monitor intended for the Compton-Hall section gives similar results. The sensitivity is adequate: for an expected dose rate of  $10^7 \text{ rad/s}$  the expected electrical signal is about 60 mV.

The dashed line in Figure 1-7 is the noise as measured on a separate shot. For this measurement the fiber and the filters were left in place, but the scintillator was removed. Clearly, the noise is quite acceptable.

The prototype version of this instrument will be tested on the DECADE module (DM1) at Physics International in the near future when a convenient opportunity arises.

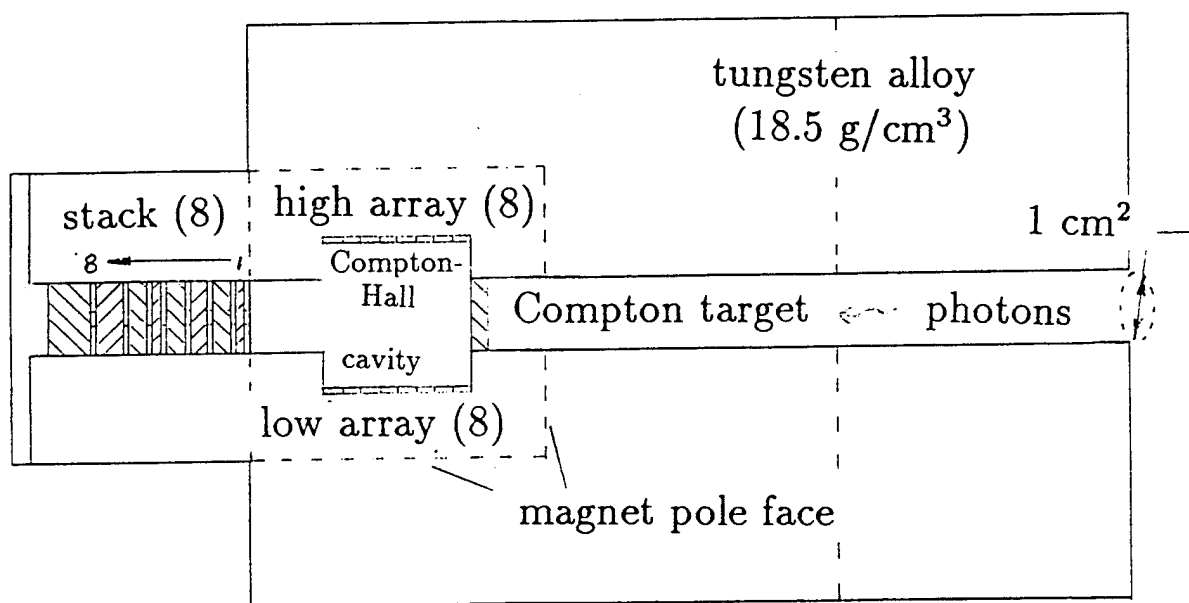


Figure 1-1. Design of the spectrometer.

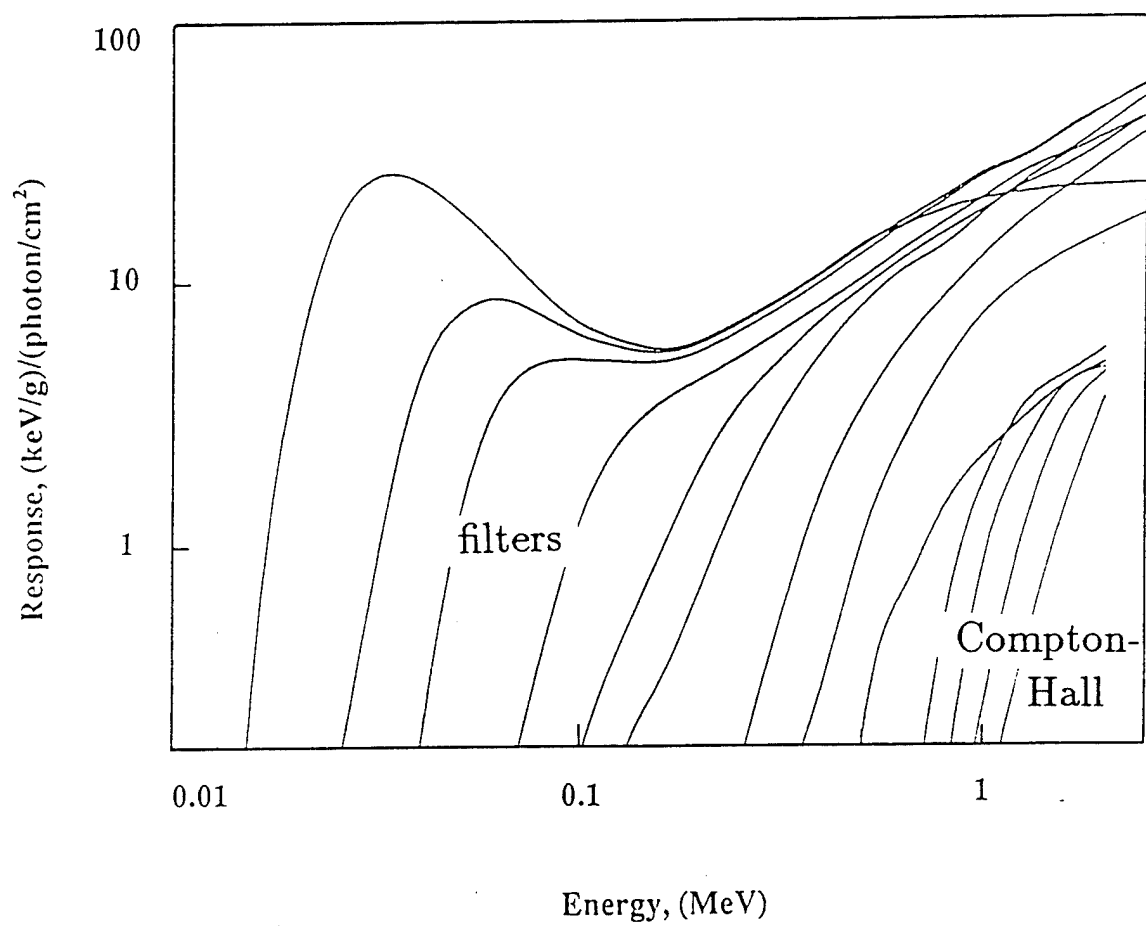


Figure 1-2. Response functions for the time-integrated spectrometer with  $\text{CaF}_2$ .

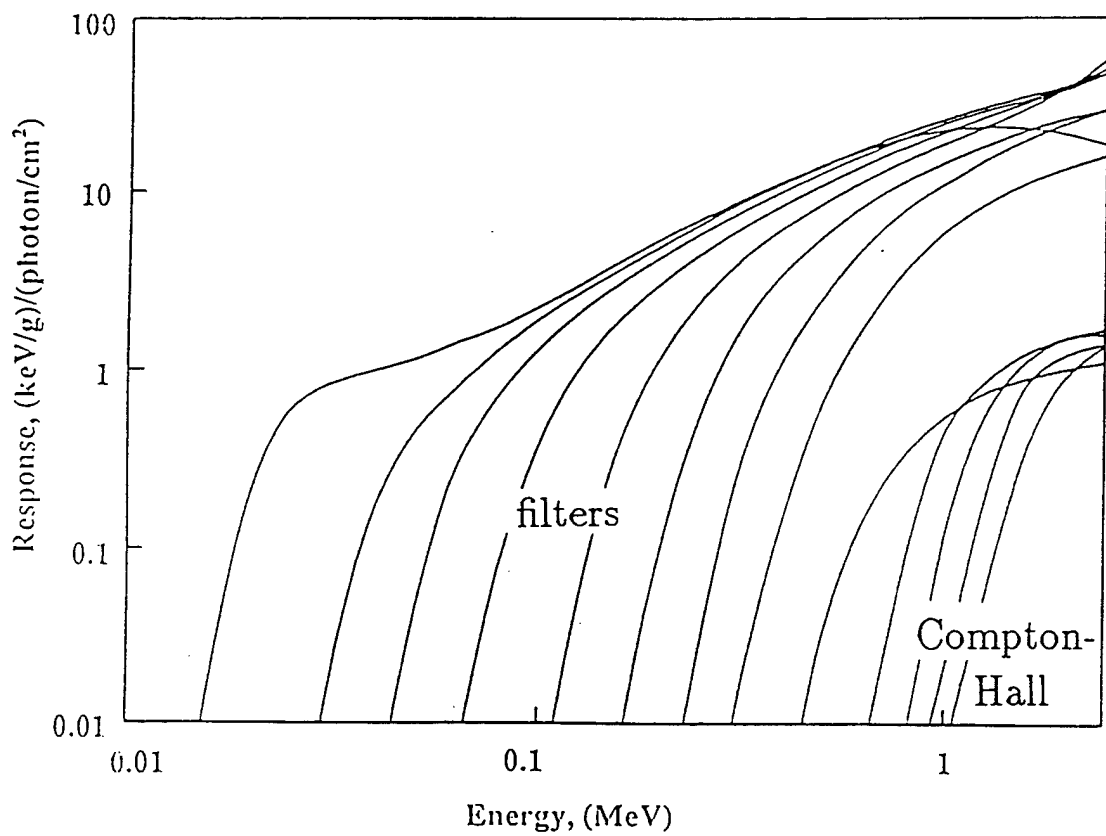


Figure 1-3. Response functions for the time-resolved spectrometer with plastic scintillator.

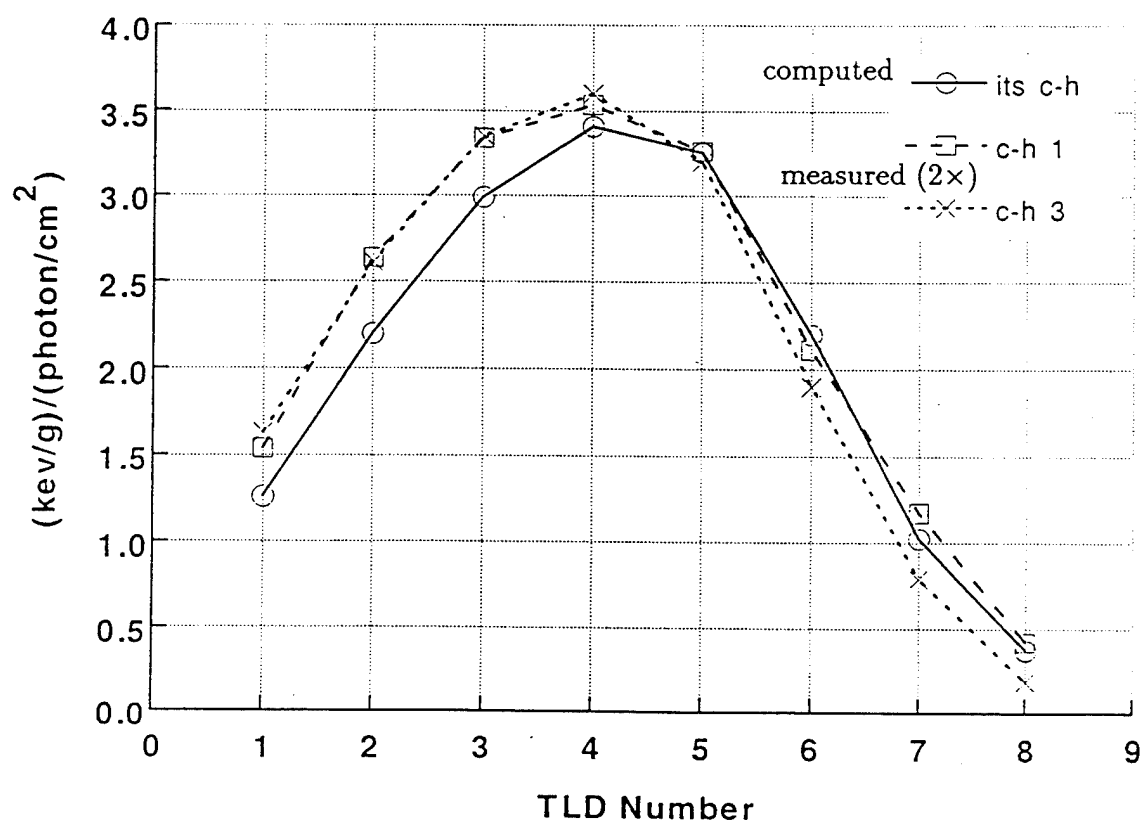


Figure 1-4. Comparison between measurements and expectations for the Compton-Hall section.

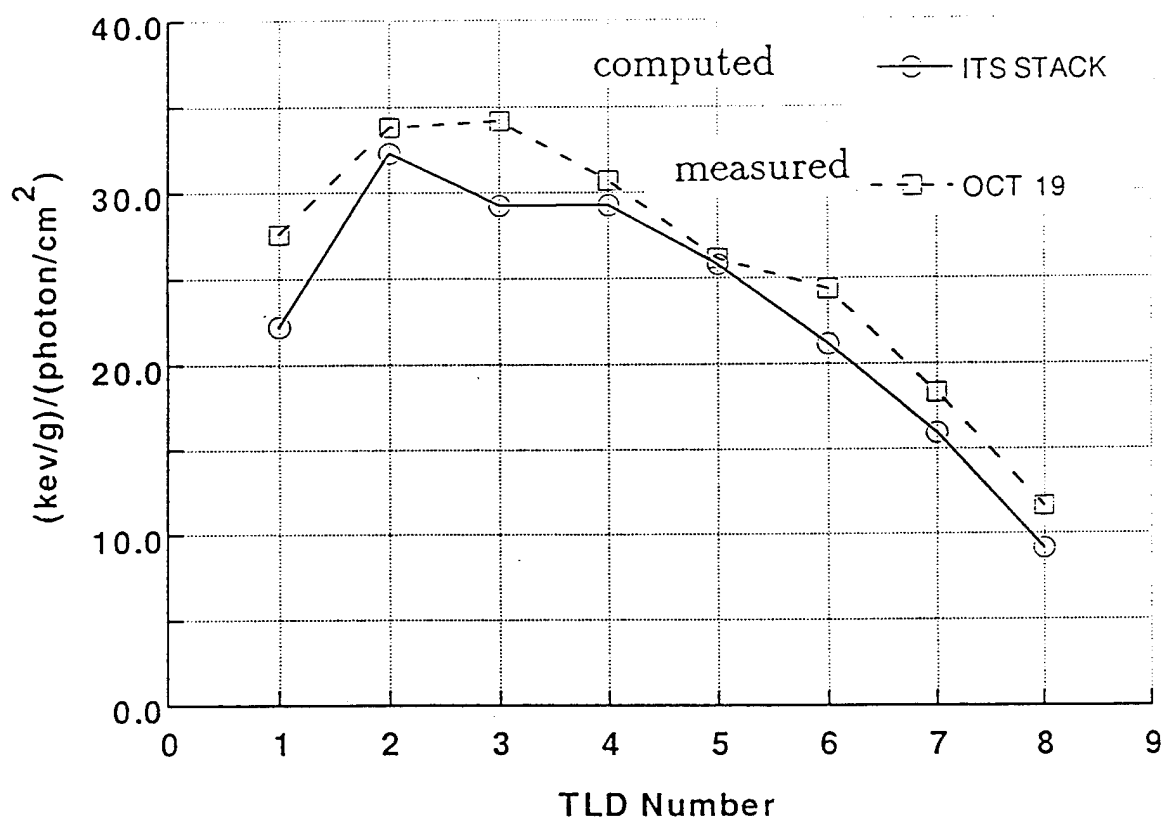


Figure 1-5. Comparison between measurements and expectations for the absorber section.

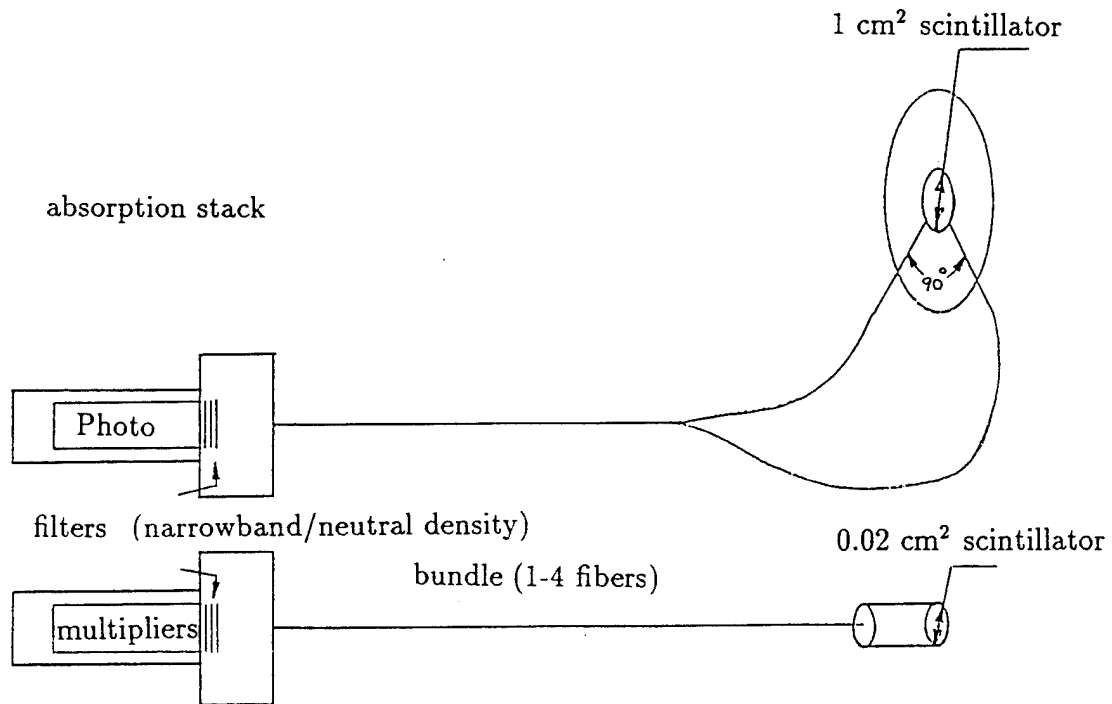


Figure 1-6. Designs of the optical scintillator-fiber dose rate monitor.

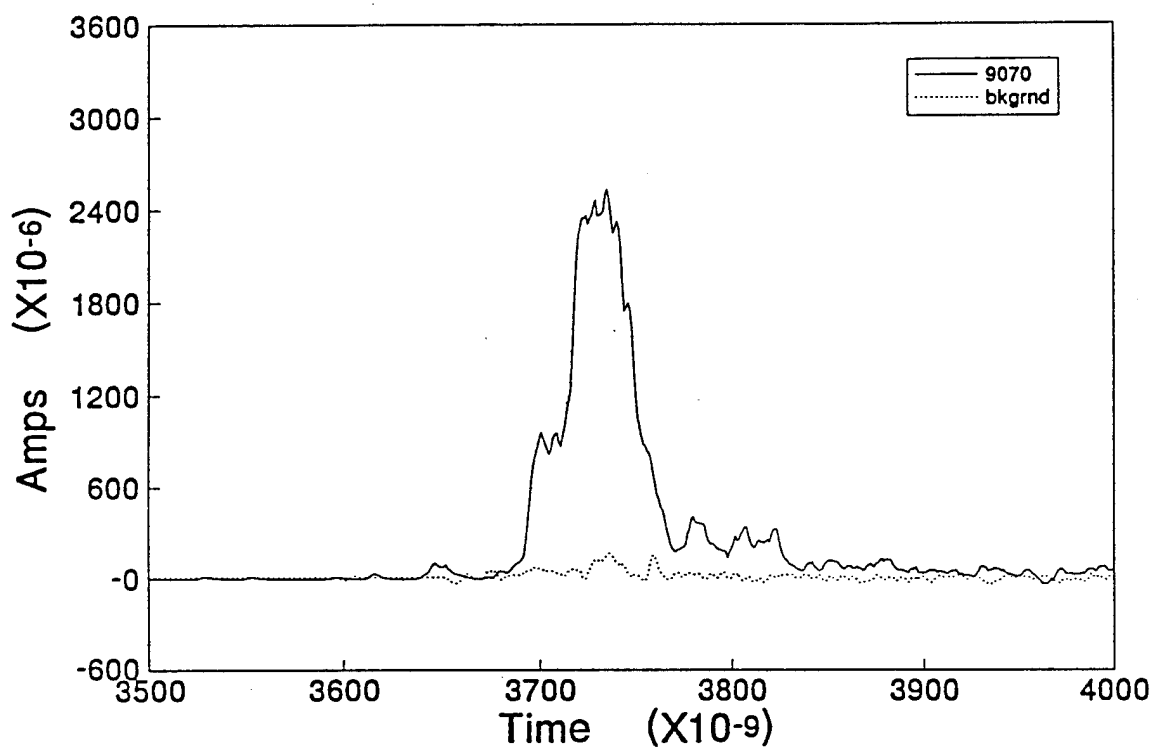


Figure 1-7. Signal produced by the optical dose rate monitor intended for the absorber stack.

## SECTION 2

### SOFT X-RAY SPECTROMETER

The time-resolved soft x-ray spectrum instrumentation was subcontracted to Physics International Company (PI). The proposed method is to couple a crystal that resolves the photon energy with a soft x-ray streak camera that supplies the time information. Although the technique is conceptually straightforward and well-known, especially in laser-produced plasma research, it has not yet been used on a PRS machine. Physics International's Dr. Failor has experience with measuring spectra from laser-produced plasmas using x-ray streak cameras. His favorite camera is an instrument developed in part for Livermore's underground test program by Kentech in the UK. Its core, the streak tube, is a rather small, light-weight package that seems ideal for interfacing with PRS machines. Powering the unit is done through cables, which go to the more bulky electronics that can be put in some convenient place. We were able to borrow such an instrument from Dr. J. Grun, NRL, for executing the preliminary tests.

As described more fully in an appendix written by PI, the measurements were quite successful. The data were taken during an ongoing shot series intended to develop a mixed argon-krypton pinch on PI's Double-Eagle. With the crystal tuned to the argon-k lines around 3 keV, and looking at the entire pinch, the signal levels in the x-ray streak camera were sufficiently large that the entrance slit could have been made an order of magnitude smaller. Equivalently, one could have looked at only an axial slice of the plasma, to look at zippering. Taking only x-rays from a radial slice through the PRS would give information about separating out plasma species during pinching. High signal levels also allow improved energy resolution.

In the past the PRS spectra from Double Eagle were sometimes resolved in time using a framing camera, the so-called MC-PIGS. Such a framing camera most likely misses short-lived phenomena. The continuous time history possible with a streak camera was chosen to get a continuous time record that could show signals as short as 0.1 ns. In the shots taken to date there is no trace of time variations this short: the fastest pulse in a specific line (see appendix) is about 1 to 2 ns wide.

Having obtained proof that an x-ray streak camera can be coupled successfully to a large PRS machine it is time to acquire such a camera for the DNA program. These x-ray streak cameras are specialty instruments, in use by only a few groups and therefore quite expensive. Prices range from about \$ 40,000 for a camera built in Russia through \$ 80,000 for the Kentech to \$ 150,000 for a Hamamatsu.

We have carefully looked at the various alternatives in streak cameras. Similar to the relatively special x-ray streak cameras are optical streak cameras. These are used extensively by Sandia National Laboratories to measure time-resolved spectra, not only directly in the optical regime but also through scintillators in the x-ray regime. DNA has a plethora of optical streak cameras that are not presently in use. These include one EG&G optical streak camera identical to the ones used by SNL, and three Thompson 506s. One of these occupies valuable space on an optical bench at SNL, while the other two are boxed up at PI. Obviously, it would be really nice if the existing optical cameras could be used

to diagnose the soft x-ray spectrum.

In principle should be possible to exchange an optical streak tube for an x-ray tube, thereby converting an optical streak camera into an soft x-ray instrument. The x-ray tube must, of course, be open to the vacuum of the PRS, or at most be closed off by a window thin enough to transmit the interesting x-rays. To maintain this vacuum the x-ray tube must have a vacuum pump, while the optical tubes are closed. For this reason the optical streak cameras are most easily (and usually) packaged as a single unit, while for interfacing with the PRS vacuum system it is handy to have the electronics separated out, as in the Kentech camera. Replacing the optical tube by an x-ray tube was tried by EG&G, but without success. Their experience shows that conversion is not so straightforward as it might seem, even though a group in at Limeil-Valenton (France), where the Thomson streak camera originated, have been able to replace optical by x-ray tubes.

SNL prefers to measure soft x-ray spectra with optical methods for various reasons. One is that access to the SNL experiments is quite difficult. Soft x-ray diagnostics demands a line of sight, which forces the instrument to be close to the machine. However, SNL's machines are quite noisy, both for radiation and electromagnetically. SNL avoids these problems by converting the desired x-rays into optical signals using fast scintillators, e.g., quenched BC 422 whose response has a FWHM of 0.25 ns. The  $\sim 400$  nm light is then carried by 10-25 m long bundles of UV-transmitting fibers to the camera in a personnel-accessible screen room.

A systematic assessment of the different options has the Kentech streak camera first on the list, followed by the lower-cost Russian camera. Converting an optical tube to x-ray use (as done by EG&G) is a distant third. The following discusses each approach in some detail, from worst to best.

The EG&G tube modification, exchanging an optical for an x-ray tube, has high technical risk. Most of the following information comes from John Radosovic, the manager of EG&G, Amador Valley, a principal contractor supporting LLNL's nuclear test program. In summary,

1. EG&G has tried making one x-ray streak tube, that apparently did not work well.
2. There is not a clear way to modify an optical tube.
3. Direct mechanical mounting of a heavy and bulky optical streak camera to a PRS machine is problematic.

The performance of EG&G's prototype x-ray tube was reportedly disappointing. At the time Keith Heinrichs was the head of the streak camera group at EG&G Amador Valley. This group built optical streak cameras for the Nuclear Test Program. Heinrichs used internal funds to build an x-ray streak tube and make some measurements using a relatively large pulsed glass laser. The x-ray streak tube was fabricated at the same facility that made the optical streak tubes, so it used the same glass envelope, and fitted in the same streak camera bodies that were used for the optical cameras. The project's funding was terminated when the work did not progress satisfactorily.

A similar project at Limeil-Valenton uses the Thomson 506 streak camera body and electronics to power two types of x-ray tubes, one open and one closed. The open tube is essential for x-rays below about 1 keV. The closed tube uses a thin beryllium foil that is not vacuum-tight, compensating for the small leak rate with a ion pump. Therefore the closed

version must be kept running on. This effort has apparently resulted in a satisfactory instrument.

A sealed streak tube is not straightforward to modify. The tube has kovar ring frit seals at three locations--the back (phosphor), the middle, and the front (photocathode). Somehow, the pressure in the tube would have to be released in a controlled manner, before the frit at the photocathode region could be separated. There is no one at EG&G Amador Valley who has done this. The original x-ray streak tube was never operated as an optical tube, and it is not clear that it could be operated in a Thomson CSF optical streak camera, although the tubes would probably be similar (RCA made the first tubes, while RTC and ITT used the RCA tubes as models). Modifying an existing tube is uncharted territory.

Mounting is easy for the Kentech camera, but difficult for either a modified optical streak camera or the Russian camera. The Kentech has a separate electrical chassis that includes the focus, bias, and sweep power supplies. On the optical camera and the Soliton/Bifo K-002 Russian camera the power supplies are mounted in the same housing as the streak tube. This makes it much more difficult to mount the camera on a vacuum system, and to rotate it at arbitrary angles. Rotation is necessary to ensure that the spectral lines run perpendicular to the photocathode input slit, in the case of the streak camera, or the gated striplines, in the case of the gated stripline MCP cameras. The Kentech camera is sufficiently light weight to be mounted directly on the diagnostic beamline without additional mechanical support. This would not be true for the other two cameras.

The mechanical mounting issue is the primary drawback of the Russian K-002 XUV streak camera, along with poorer background discrimination due to the use of a MCP photocathode. If the quoted characteristics of the camera are accurate, the sensitivity range ( $0.01 \text{ keV} \lesssim h\nu \lesssim 1000 \text{ keV}$ ), temporal resolution (200 ps), linear sweep range ( $1 \text{ ns} \lesssim t \lesssim 100 \text{ ns}$ ), and frame exposure time ( $5 \text{ ns} \lesssim \tau \lesssim 100 \text{ ns}$ ) would be acceptable, although the time resolution is limited by the temporal dispersion of the MCP photocathode. Moreover, replacement MCP photocathodes would be expensive, since they are nominally coated with different photocathode materials. Presumably, the builders could put in, on request, a foil photocathode as in the Kentech camera, at least if the sensitivity remains acceptable.

Another drawback is the sensitivity of a MCP photocathode to high energy x-rays. The Kentech avoids this by using a thin transmission photocathode that is much less sensitive to hard x-rays ( $40 \text{ keV} \lesssim h\nu \lesssim 1500 \text{ keV}$ ). Because of their high sensitivity to hard x-rays, MCP photocathodes are used in the bremsstrahlung framing camera at the SNL/ABQ Saturn facility.

The MCP gain stage of the streak camera is likely the primary source of noise in these streak cameras, whether they be optical or x-ray. For this reason, x-ray streak cameras should not be ruled out in harsh hard x-ray environments, like the Saturn or Decade facilities. In the case of an optical streak camera, the light would be fiber optically coupled from a fast scintillator to the photocathode of the optical streak camera. In the case of the x-ray streak camera, the fiber optic would be coupled instead from the phosphor output of the streak tube to the photocathode input of the MCP intensifier. In both cases the hard x-ray sensitive MCP would be shielded from the hard x-rays.

As is known, transmission x-ray photocathodes have instantaneous time response on

a picosecond timescale, while "fast" scintillators are limited to about 0.25 ns. For this reason we initially rejected SNL's scintillator/fiber/optical streak approach. As it turns out, the timescale of each of the spectral lines measured so far is at least 1 ns. All these lines would be seen quite accurately through scintillators.

Direct registration of the x-rays is not only faster, but also more sensitive, resulting in a better signal to noise ratio. However, Double-Eagle's PRS gives about one order of magnitude higher signal than needed by the Kentech camera. Such a signal level is sufficient for the scintillator/fiber/optical streak approach. Instead of working at the edge of the instrumentational sensitivity, we would like to use the excess signal for putting in axially or radially resolving slits, and for keeping the noise down.

The estimates go as follows. For example, a 30 nm gold x-ray cathode produces only about 0.06 electrons per 3 keV photon or 0.02 mA/W (Henke, J. Appl. Phys **53**, 1509). Although optical photocathodes are more energy-efficient, about 0.23 electrons or 70 mA/W for a typical 3.35 eV photon (370 nm) from a fast scintillator such as quenched Bicron 422, but the efficiency of the complicated conversion chain uses up this efficiency.

Not all x-rays are absorbed. To avoid spatial smearing the scintillator can not be thicker than about 60  $\mu$ m. Such a thin plastic scintillator absorbs only 20% of the x-rays. In a quenched scintillator the energy conversion efficiency from x-rays to photons is necessarily low, for Bicron-422Q about 0.006. This corresponds to one absorbed 3 keV x-ray giving 5 photons, or 1 photon per incoming x-ray. The energy efficiency of these combined processes is obviously very low, only about 0.1%.

Photons come out isotropically, and only a small fraction can be captured even with a reasonably efficient optical system. For example, with a f/1 lens at 1:1 magnification this fraction is about 1.6%. The total efficiency is then about  $0.016 \times 0.23 \simeq 0.004$  electrons per x-ray photon, about 7% of the number of electrons per x-ray photon from an x-ray cathode.

It is possible to improve on the different efficiencies, usually at some cost in another parameter. For example, a 100 nm thick CsI x-ray photocathode is an order of magnitude more sensitive than 30 nm gold, but CsI is much harder to work with. We have enough signal, and prefer gold. Likewise, the efficiencies in the optical chain can be increased, e.g., the capture efficiency can increase from 1.6% to 5% or more by using fiberoptics instead of lenses, but with some loss in spatial resolution. With a more efficient optical chain the optical streak cameras might still be useful for diagnosing the spatially averaged x-ray spectrum.

The consensus from these various analyses is that a direct registration x-ray streak camera is preferred, largely because it promises to provide higher quality data than the circuitous route through a scintillator/fiber/optical streak. Of the direct soft x-ray cameras looked at, the Kentech is favored over the Russian camera on grounds of convenience and technical risk, even though the Russian camera offers excellent value for money.

The proposed budget contains \$ 110,000 for an appropriate version of the Kentech camera. At this time (October 30) we have decided to proceed with the purchase of the most basic Kentech x-ray streak camera, and to add an electronic readout as a separate effort later.

### SECTION 3 VOLTMETER

Of the different diagnostics the ion range volt meter has received the least emphasis to date. There are various reasons for this, all related to the availability of suitable dose rate detectors. The voltmeter needs various (10-20) parallel channels of dose rate data. In principle, the instrument could use the same dose rate detector as the hard x-ray spectrometer, but this detector is still under development. The originally proposed detector is one of DNA's four available optical streak cameras. These cameras are being transferred to our work, but they have not yet arrived. A final reason is that the volt meter does not seem to be in the critical path for DNA's DECADE generator. Instead, DECADE's voltage will be estimated from the hard x-ray spectrum, which is to be measured with the time-resolved spectrometer built earlier for NSWC.

A time-integrated version of the volt meter is complete. The approach is simple. A time-integrated detector looks at the dose from ions that have penetrated different thicknesses of foils, here aluminum. The dose profile can be unfolded in terms of the ion energy spectrum. The peak in the ion energy spectrum is the voltage. Previously, the time-integrated hard x-ray spectrometer with a time-integrated dose diagnostic (ThermoLuminescent Detectors or TLDs) becomes a time-resolved hard x-ray spectrometer by replacing the TLDs with GaAs PhotoConductive Detectors (PCDs) that measure dose rate. Likewise, to get the temporal profile of the voltage one simply replaces the dose measurement with a dose rate measurement.

It should be pointed out explicitly that the depth-dose profile, both the time-integrated and the time-resolved versions, are directly useful in ion beam tests of thermostructural response. In fact, the proposed voltmeter was inspired by the way wherein we measured the ion spectrum on DNA's Aurora simulator at the Army Research Laboratory, DNA's ideal machine for this purpose. Two equivalent methods can be used to measure the dose profile, stacked foils or a wedge filter. Dr. G. Merkel (ARL) uses the stacked foil method exclusively for his diagnostics of ion beam fluence and energy. Dr. F. Young at NRL prefers a variant of the wedge filter technique. Obviously, we have implemented the wedge filter method on Aurora's ion beam, because the method is identical to a time-integrated ion range volt meter. The time-integrated instrument can then be directly converted into the time-resolved volt meter once the dose rate monitor becomes available.

The time-resolved volt meter is useful to the ion beam test community because it measures the depth-dose profile directly as function of time. This measurement is needed to ensure that the impulse from the instantaneous heating by the ion beam stays below certain desirable limits. This need motivated Dr. Merkel to develop such an instrument. His version uses individual filters in front of diamond photoconductive detectors (PCDs), and conventional digitizers. The paper describing his results should be finished before CY'96.

We intend to use an all-optical scintillator/fiber approach. The initial readout will be with photomultipliers as done previously on PBFA-II at Sandia National Laboratories by J. Bailey, A. L. Carlson, T. R. Lockner, and J. Maenchen around 1988. They did

not publish their work. The only written version is a draft paper entitled *Time-resolved voltage measurements on PBFA-II using a range filter-scintillator diagnostic*. However, if more channels are needed than about 10 or so, the the best instrument to register the optical signal is an optical streak camera. The principal proviso is that the signal strength is sufficient. Our estimates have shown that signal strength should not be a problem. We are anxiously awaiting the arrival of the optical streak cameras to verify this point.

An annoying feature of the time-integrated ion range volt meter or its equivalent, the wedge filter method of measuring the depth-dose profile in ion beam tests, is reading out the data. The dose diagnostic, thin radiachromic foils, must be placed by hand in a reader that measures their transmission. A known calibration converts from optical density to dose. The optical transmission can be measured in a traditional (analog) fashion, or digitally interfaced to a computer.

The standard reader for radiachromic foils uses standard  $1\text{ cm}^2$  pieces to look at a 3 mm radius spot in the center. The remainder of the foil is exposed, but not read. Ten to 20 foils must be read to get the spectrum, a time-consuming procedure because the foils are very thin ( $\sim 10\text{ }\mu\text{m}$ ) and difficult to handle. It would be much better if the ion energy spectrum could be found from information on a single foil. For a time-resolved instrument the equivalent is to find the dose rate from the light emitted by a scintillator just in front of the fiber, as we intend to do.

The short range of  $\sim\text{MeV}$  ions makes it possible to expose small spots quite precisely. Therefore a single  $1\text{ cm}^2$  foil could register the dose behind many different filters. Figure 3-1 shows the construction of an appropriate filter stack, and a radiachromic foil exposure using Aurora's ion beam. The transition between different thicknesses of filters, each  $4\text{ mg/cm}^2$  aluminum, is seen at the edge of the picture thanks to a supporting grid.

The picture must now be read with better spatial precision than available in the standard radiachromic film reader. NSWC's ion beam group at NSWC has available a densitometer that uses an optical fiber to localize the measurement, but unfortunately the equipment no longer works. No one wants to fix it because the original motivation for the instrument's use has disappeared.

The film reading method with the most promise is to use a microdensitometer. This is an expensive but standard instrument that is commonly available at many laboratories, including NSWC, NRL and ARL. The microdensitometer is designed to scan film, i.e., to determine the optical density of film with high accuracy and good spatial resolution. Typically, microdensitometers measure the optical density over three orders of magnitude in spot sizes of 10 or  $25\text{ }\mu\text{m}$ , ideal for reading radiachromic film. Commonly the microdensitometers use white light, but radiachromic film is best read with yellow light (600-610 nm). Most microdensitometers have built-in filters, but none of these is for the desired band. Therefore, a filter must be placed externally. These filters should be available, but we have yet to locate them.

In normal operation the data from the microdensitometer are stored on a computer, to be read by specially developed programs that are optimized for each particular application. We have written a program to take the optical density of radiachromic film behind a film stack from the microdensitometer, and to read out the optical density over designated areas. This density is then converted into dose for further transmission to the spectral

unfold program.

Up to now we have not been able to make full use of this measurement chain, largely because Aurora's ion beam is no longer working and we can no longer take measurements in a convenient manner. Moreover, the few sample foils that we took data with were scanned by mistake with a filter that absorbs in the same band as the foil. Therefore these samples gave no useful data.

Presently, the holdup in the voltmeter work is the optical dose rate detector. The shortest way to this goal is to get the scintillator/fiber/photomultiplier chain working for use on the time-resolved hard x-ray spectrometer. This dose rate diagnostic should transfer without change to the ion range volt meter. Aurora's unfortunate demise forces us to find alternative places to exercise the diagnostic. We are exploring options at NRL and DM1. Gamble II creates ion beams intentionally and DM1 unintentionally. In fact, ion depth measurements could be a welcome accessory diagnostic in the DM1 assessment effort.

A completely different but still crucial aspect of the volt meter is conversion of depth-dose data into the ion energy spectrum. We have rewritten the code used for this purpose. This code, YOGI, takes some reasonable initial ion energy spectrum, and computes the expected dose as function of depth for this spectrum from the theoretical dose as function of depth for monoenergetic ions. Then the code changes the spectrum in a random way until the computed doses at the different depths match the measured depth-dose profile. Essentially the same code is used to unfold the hard x-ray spectra from the dose or dose rate behind different filters. The method is described in S. G. Gorbics and N. R. Pereira, *Differential absorption spectrometer for pulsed bremsstrahlung*, Rev. Sci. Instrum. **64**, 1835 (1993).

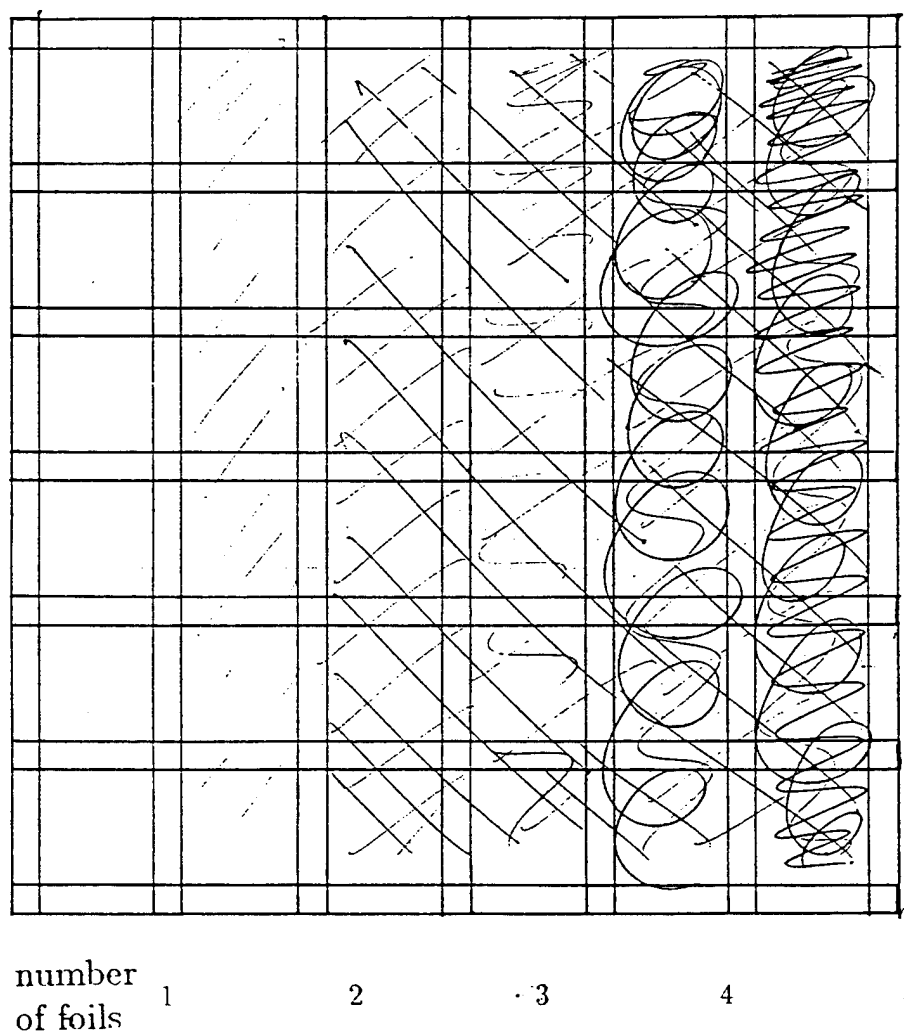
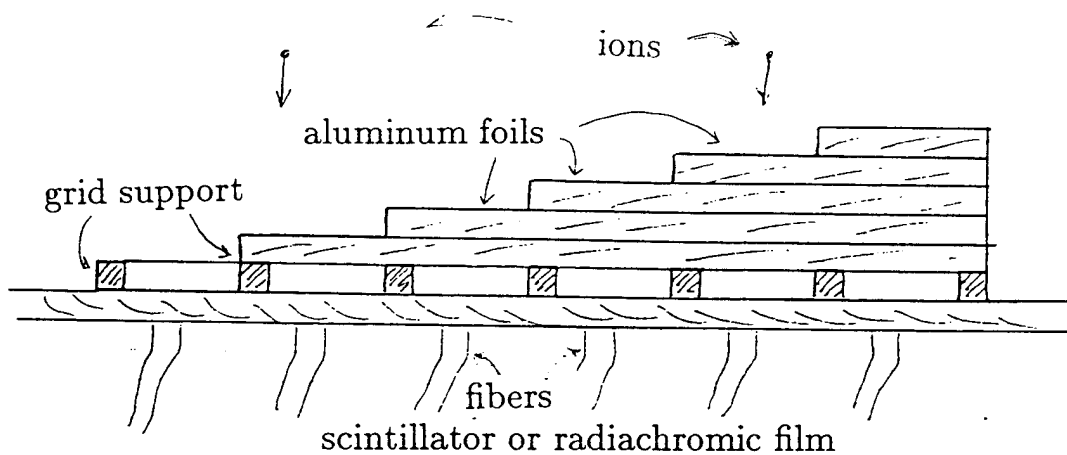


Figure 3-1. Construction of the filter stack for the volt meter.

## SECTION 4

### DEBRIS

Our concept for a debris diagnostic is similar to the filtered hard x-ray spectrometer, and also to the ion range volt meter. In the spectrometer different x-ray filters transmit ever-decreasing fractions of the incoming radiation, and from these differences the spectrum is unfolded. For x-rays the filters are multiples of 1/16 inch thick layers of different elements. The thickest layer is about 6 mm thick tungsten to discriminate against  $\sim 0.5$  MeV photons. Likewise, filters of increasing thickness separate out ions of different energies. Unfolding gives the ions' energy spectrum, and therefore the peak energy. Now the filters at most 0.1 mm of aluminum for  $\sim 5$  MeV ions, much thinner because ions do not penetrate so easily into materials.

The debris diagnostic is also a stack of thin foils. The thinnest debris shields are typically about  $25\text{ }\mu\text{m}$  (1 mil) or at most  $50\text{ }\mu\text{m}$  thick. Therefore the penetration depth of typical debris is on this order or less. The differentiating foils must be even thinner, a fraction of 1 mil. The thinnest material conveniently available is  $2\text{ }\mu\text{m}$  aluminized mylar. A stack of up to 40 of these foils have been exposed to the x-rays and the debris from a typical aluminum pinch on Phoenix.

The results are as follows. Typically, the first 10 foils are evaporated, while foils 11 to 15 show decreasing amounts of holes. From foil 16 onwards no more holes are evident when the foils are held up to the light. Apparently, debris does not penetrate further than about  $30\text{ }\mu\text{m}$  in stacked layers of aluminized mylar.

The raw measurement is rather straightforward, but the interpretation of the data in terms of debris size and speed is much more difficult. To find these it is necessary to verify that the holes in subsequent foils line up, and to measure quantitatively the number of holes as a function of depth. The next ingredient is the equivalent of the response functions: what is the penetration depth of spherical particles as function of debris mass and speed, and the parameters of the foil, mass per unit area and perhaps material strength. Unfolding would then give the analogy of the spectrum, some distribution of mass and speed of the debris particles.

The energy and size distribution of the debris is particularly interesting because energy and size determine the minimum thickness of the debris shield. Detailed information on the debris is only needed to estimate its penetrating power, not for anything else. At some point later the data might be compared to predictions from a model for debris generation. Under another effort we have developed a conceptual model that is not yet good enough for quantitative predictions.

The model assumes that the debris consists of evaporated material from the current return electrodes, and also from the places where the electrical current enters anode and cathode. The material evaporates by resistive heating, and also from x-ray irradiation. These processes determine the size distribution of the debris, in a still mysterious manner.

In the model the debris gets its velocity from the expansion of the pinch. The PRS is a column of hot gas. Its material is the original pinch mass, possibly mixed with additional

material from the electrodes, and its temperature is sufficient to give approximately the maximum magnetic pressure during the pinch. Without magnetic pressure, after the current pulse is over, the gas column must expand. The expanding gas drives the debris out of the pinch region. A qualitative prediction is that all debris has been accelerated by the same amount of mass expanding from the pinch region. This leads to an inverse correlation between velocity and size, with the larger debris particles moving slower and the smaller particles moving faster.

The same argument in reverse suggests that the debris can be stopped by about the same amount of material irrespective of its size. Smaller particles of a given velocity penetrate less than larger particles with the same speed. However, the smaller particles are faster, and the larger would exactly compensate for the higher penetration strength of the larger particles.

It seems superfluous to determine the velocity and mass distribution of the debris, only to turn around and use these data to determine how far the debris penetrates. It is much simpler to measure debris penetration directly, and leave it at that. The diagnostic here does exactly this minimum amount needed for debris shield design.

Further development of the debris diagnostic was deferred once it became clear that the debris foil stack measurement directly gives the most interesting quantity, namely the debris shield thickness. Debris penetration in a foil stack avoids uncertainties from an indirect measurement of the debris itself, and equally uncertain penetration into a material to be given by theory. These complicated problems would have to be dealt with in attempts to measure debris speed and size by other methods such as laser scattering. Such measurements are much harder to make, and less certain in their predictions for the required thickness of the debris shield. Laser-based debris measurements are explicitly called out under another effort.

Besides the size and speed of debris particles the pinch produces other undesirable emanations. One is fast electrons, the other a pulse of hot gas, with an as yet uncertain pressure and speed.

To my knowledge fast electrons were identified for the first time by Dr. F. Davies of K-Tech. He used PVDF pressure gauges on Saturn. An early spike simultaneous with the pulse arrival time was first attributed to bremsstrahlung. However, the early pulse is strongly reduced by putting a sweeper magnet in front of the PVDF, hence the identification as fast electrons. We found the same early pulse on Phoenix, but we did not have the occasion to repeat Davies' experiment with the sweeper magnet.

The fast electrons affect not only a pressure measurement, but also the debris shield. Therefore, the debris shield might be heated somewhat by these electrons. Conversely, whatever heating there is could be prevented by a sweeper magnet.

In a test of this setup the sweeper magnet did not seem to reduce the heating noticeably. Instead, it appeared that the first 10 foils were heated more than before. The suspected reason is stagnation of the hot gas in the throat of the magnet. The front foils evaporate. The hot gas from evaporation of the foils encounters hot gas from the pinch that flows in the opposite direction. In this experimental setup the foils were behind a cylindrical enclosure for the magnet. The evaporated gases could not escape, resulting in increased heating. With an escape path for the hot gas the number of evaporated foils

seems to decrease, but not by much. At this time the situation is still ambiguous.

"Hot gas" as used here is an evocative term for material that should be expected to come from the pinch region after the current pulse is over. Hot gas may be the pinch material itself, or material from the cathode and/or anode: this hot gas accelerates debris particles. The gas is fast, but has relatively low density. In addition, "hot gas" may include much cooler and slower but possibly denser gas, perhaps electrode remnants or gases evolving from electrode surfaces. We do not know of a measurement of the pressure over the hundreds of  $\mu\text{s}$  after pinch time that such gases may affect debris shields.

The lesson from these tests includes not only the minimum thickness for the foil needed to stop debris particles, but also as another indication that additional influences, such as hot gases, may be important in keeping debris shields survivable. We suspect that debris shields fail because they are weakened by x-ray heating, and then overstressed where debris hits. The subsequent pulse from the hot gas is then too much to take, and the shield fails. Preventing or at least minimizing impact from hot gas might protect the debris shield.

## SECTION 5

### CURRENT PROBE

The high linear current density diagnostic to be developed under this contract was based on previous work done in part by Dr. K. Struve (Mission Research Corp.) at Sandia National Laboratories for their Saturn PRS machine. Obviously, the most efficient execution of this work is through a subcontract to MRC for Dr. Struve. He would develop a method to infer the current from the magnetic pressure and the resulting shock launched into a material. Polyvinylidene Fluoride (PVDF), a plastic that can be made with a predictable electrical polarization, would convert the shock into an electrical signal.

Unfortunately, delays in the paperwork did not allow Dr. Struve to commence work as originally intended. This delay turned out to be a blessing in disguise, because in this time but under another program Dr. Struve has developed a standard  $\dot{B}$  loop to a high degree of sophistication. Equally important, through other work we became aware of hitherto unrecognized problems in diagnosing electrical current from its shock, and in using PVDF pressure sensors. In addition, some practical problems appeared to make the PVDF-based pressure measurement technique less suitable for part of the probe's intended use, as routine current monitors on DNA's operational simulators.

For the latter purpose a major difficulty with the PVDF shock probes is that the probes are not reusable even in the relatively benign parameter regime of most interest, namely magnetic pressures that do not destroy the machine's front end. This limit is roughly the tensile strength of common materials such as aluminum (about 200 MPa) or stainless steel (500 MPa). Already at a much lower pressure the piezoelectric material does not revert to its original polarization state. PVDF's beauty is that during the fabrication process the material acquires a specific electrical polarization, which determines the calibration of the probe theoretically. Unfortunately, the desired current per unit length gives a pressure pulse that exceeds the threshold for changes in polarization. For the next shot the probe's calibration has changed. Worse, a calibration shot may affect the calibration of the next shot. For a routine diagnostic this is unacceptable.

The desired current per unit length corresponds to a PRS pinch with peak current  $I \simeq 4$  MA, as available now on various DNA machines, to  $I \simeq 20$  MA for a future DECADE PRS machine. According to the Statement of Work the measurement location is to within a radius  $r \simeq 0.3$  m from the load for the 20 MA pinch. For the DECADE pinch the minimum current per unit length is then  $I/2\pi r \simeq 10$  MA/m, and the magnetic field is  $B \simeq \mu_0 I/2\pi r \simeq 12$  T. The corresponding peak pressure is 60 MPa, which is higher than the depolarization threshold for PVDF.

Therefore the PVDF-based sensors are inherently one-shot devices, and they are unsuitable for routine use on operational simulators. Instead, their proper place is as a means to monitor the highest possible linear current densities in a research environment, where each shot is allowed to destroy the probe physically. Another niche is where excessive electromagnetic noise must be avoided. Pressure-based probes have a built-in delay from to a shock transit time. The intended work on PVDF probes is discussed further below.

Besides the depolarization problem there are some classical electromagnetic issues

that affect the desirability of pressure probes as an electrical diagnostic. One of these is current penetration into the material, i.e., the diffusion of the magnetic field into the material. Penetration of the current can be up to 0.3 mm during a nominally 200 ns pulse. Especially bothersome would be nonlinear effects i.e., the diffusion of the magnetic field as affected by changes in the electrical resistivity and similar transport coefficients (such as thermal conductivity).

Figure 5-1 illustrates the effect, using parameters typical for a PRS shot on Phoenix as used in our studies of debris generation. The solid line is the current density at 40 ns and 80 ns into a return current rod, when the current is about 2 MA and 3.5 MA. With constant electrical resistivity  $\eta = \eta_0$  the current profile is purely exponential. However, when the resistivity can change with temperature  $T$ ,  $\eta = \eta(T)$ , the current penetrates deeper, and the profiles are longer exponential (dashed lines). As a result, the  $j \times B$  force that produces the shock also changes shape, from an exponential to something more complicated. The annoying thing here is that the shock starts to depend on many parameters, such as the temperature coefficient of resistivity, that may not be sufficiently well-known for the particular material of interest. These and similar problems would make interpretation of the probe's signals difficult.

Partly in recognition of these various issues surrounding PVDF pressure sensors, Dr. Struve has developed during the first year a traditional shielded  $\dot{B}$  probe into a sensor that works at the desired current per unit length. This shielded  $\dot{B}$  current probe fulfills the Statement of Work under the present contract. The probe is scheduled to be tested on ACE 4 in the near future. Once these measurements work to his satisfaction Dr. Struve will return to developing shock measurement into a diagnostic for still higher current densities, where any sensor (including the  $\dot{B}$ s) would be destroyed by the shock from the magnetic pressure.

The highest linear current density achieved with the shielded  $\dot{B}$ s is 40 MA/m, obtained within 3 cm of the pinch on SNL's Saturn. On Saturn the peak current is 8 MA, and the peak magnetic field is about 50 T. The corresponding peak pressure is 1 GPa (10 kBar). Still larger currents per unit length could occur at a similar distance to the pinch on the 20 MA DECADE PRS machine (or on SNL's PBFA-Z). Currents per unit length exceeding about 40 MA/m are the proper target for the pressure-based diagnostics.

For a pressure probe the limit to the shock pressure is the Hugoniot Elastic Limit (HEL). Higher pressure produces nonlinear shocks that are hard to interpret. After the shock the material is distorted, and a possible second shock would behave differently. However, for such strong shocks the hardware does not survive, and the probe does not either.

The pressure limit is quite high. For example, tungsten's HEL is 3.7 GPa and sapphire's HEL is 20 GPa. Typically, the HEL  $P_H$  is a few times larger than the tensile strength  $P_t$ . For an ideal material  $P_H \simeq 2(1 - \nu)/(1 - 2\nu)P_t$ , where  $\nu$  is the Poisson ratio. For most materials  $\nu \simeq 0.3$  and  $2(1 - \nu)/(1 - 2\nu) \simeq 3.5$ . The formula is approximate: for a specific steel of tensile strength 0.6 GPa the HEL is 1.9 GPa,  $3.2 \times$  larger than the tensile strength but not  $3.5 \times$ . In any case, the pressure probes can monitor the current in parameter regimes where they can not survive mechanically. Careful mechanical design of probes to reduce the pressure through acoustic mismatches is needed to create a monitor

for the highest currents per unit length. Sapphire's HEL corresponds to 200 MA/m, DECADE's anticipated current at 1.5 cm from a PRS.

Figure 5-2 shows the signal from a standard PVDF probe intended to measure shocks from debris on plasma radiation sources. The shock in this case comes from a calibration setup at SNL. A 3 ns long laser pulse evaporates a thin layer of aerodag sprayed on the front face of a lexan shock transmitter to the PVDF, which is attached on the back side. Behind the PVDF is another sheet of lexan. The time scale is 100 ns/div, with the beginning of the trace at the shock time.

About 580 ns after the laser pulse the shock arrives at the PVDF. As seen in Figure 5-2b, the shock generates a -14 V peak negative pulse (this trace was taken with 10× attenuation and 1 V/div). The electrical pulse from the PVDF is about 10 ns, wider than expected from the shock the probe is trying to measure. After the negative pulse there is a positive pulse. In the ideal case the positive pulse should be a reflection of the negative pulse, but it is not: the amplitude is about half, 7 V, and the width is also larger, up to perhaps 15 ns. A detailed analysis of these and similar traces, to be performed later on, might confirm that the difference is due to imperfections in shock propagation. Possible culprits besides nonlinearities include unintended mismatches as seen best on the unattenuated trace in Figure 5-2a. The small hiccup at 620 ns suggests a mismatch between the PVDF and its surroundings.

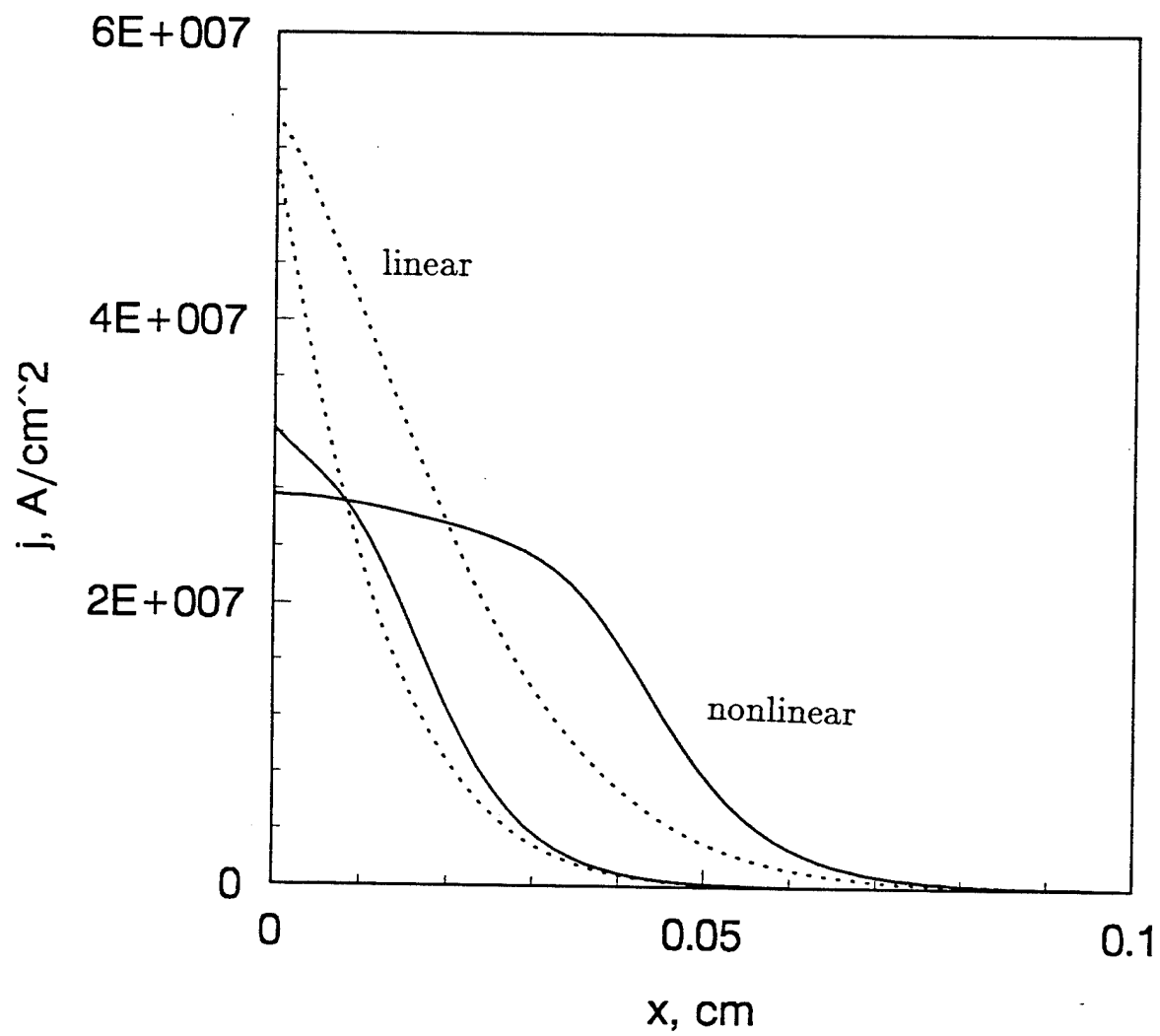
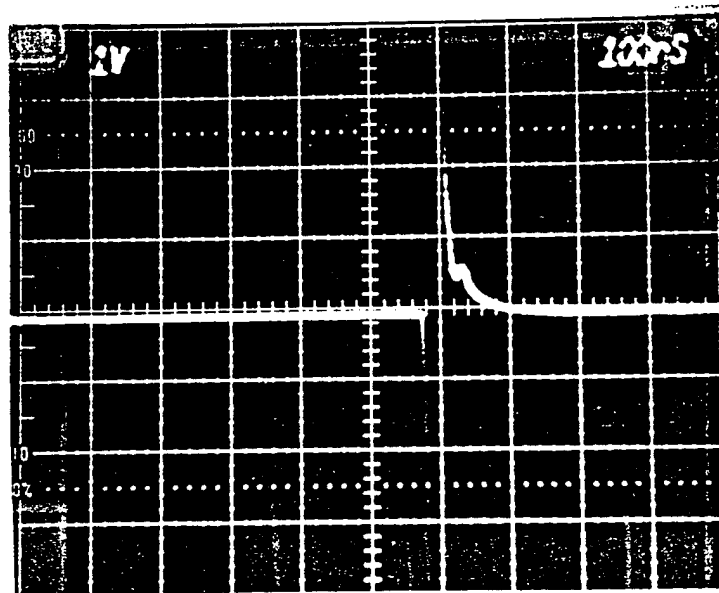
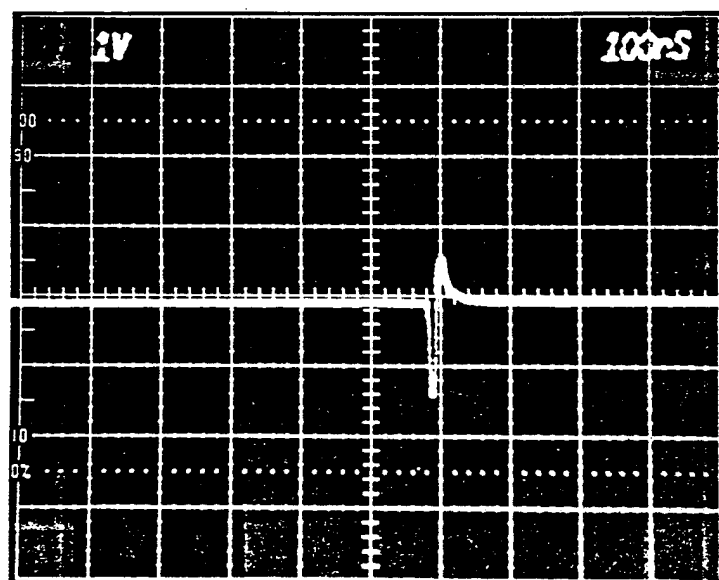


Figure 5-1. Current profile with linear and nonlinear penetration at 40 ns and 80 ns.



a



b

Figure 5-2. Signal from a PVDF sensor with a laser-driven shock.

**APPENDIX**  
**X-RAY STREAK CAMERA**

For measuring time-resolved x-ray spectra with an x-ray streak camera the primary goal in the first year was to demonstrate feasibility of the proposed approach. This goal was achieved, and the data obtained illustrates the benefits of using a streak camera to record the time evolution of the x-ray spectrum, namely (1) sub-100 ps time resolution, (2) large dynamic range, and (3) continuous spectral records. This diagnostic will be invaluable in measuring the dynamics of Mg-coated Al wire arrays during an experimental campaign planned for early 1996. It can also be used in the determination of stability of long implosion time PRS loads proposed for ACE-4.

**Experimental Setup**  
To demonstrate the camera, we used a spectrometer fixture built under a previous DNA program, and borrowed a streak camera from Jacob Grun of NRL. The physical layout of the measurement is shown in Figure A-1. This spectrometer design was used for a number of reasons:

1. It could accommodate the relatively large diameter streak camera front end.
2. A hermetic seal protects the HV streak tube from the poor vacuum that results when the gas puff fires.
3. The Bragg diffracting crystal can be positioned accurately externally, without having to bring the streak camera up to air.

The hermetic seal was provided by a 3 mil thickness of kapton, and an additional 8 microns of aluminized kapton was installed in the filter box. A curved PET crystal was used to disperse the spectrum, and 8 microns of aluminized kapton was installed as a fluorescent shield. A 50 nm thin gold transmission photocathode supported by 2  $\mu\text{m}$  thick mylar converted the x-rays to electrons that were swept by the streak tube. The sweep speed was set to 870 ps/mm, the slowest speed provided by the sweep supply. The streak camera intensifier was operated at one notch below highest gain. These settings produced satisfactory streak images, such as the one shown in Figure A-2. Here the horizontal axis is the photon energy, from about 3 keV at the left to 4 keV to the right. The vertical axis is time, increasing upwards, with the scale given by the bar. The zero time is arbitrary: the maximum in the lines coincides with the pinch time. This shot, Double eagle 3391, did not use an entrance slit to the spectrometer, so that the spectrum is averaged over the entire pinch (the streak camera has a slit, of course).

The most striking feature of the data is the relatively slow rise and rapid fall of the x-ray pulse. This can be seen from the  $\text{Ly}_\alpha$  line in the streak record shown in figure A-2. In Figure A-3, a plot of the spectrum at peak compression illustrates the moderate energy resolution and high dynamic range of the instrument. Analysis of the spectra will provide estimates of the electron density and temperature time evolution.

The streak records compare favorably with the standard PRS diagnostics. A comparison between a photoconductor detector (PCD) and the streak record of the argon  $\text{He}_\alpha$  line is shown in Figure A-4. The data points for the PCD are indicated by the + signs. These points are separated by 1 ns. The streak record was digitized at less than 100 ps per point. The streak camera measurement shows good agreement except for a more rapid rise and a much more rapid fall that can not be registered by the PCD.

The x-ray emission from higher ionization states show an even more rapid time response. This is illustrated in Figure A-5. The Lyman or hydrogen-like emission rises

and falls more rapidly than the helium-like. Thus the temperature ramps up relatively gradually, but drops rapidly after peak emission. The relatively slow ramp up of emission is consistent with the compression of a lower density core by a denser shell.

Future plans include the fabrication and fielding of a dedicated streak camera spectrometer. Our goal is to have the spectrometer fabricated by the end of March, 1996, so it can be fielded at Double EAGLE. The dedicated spectrometer will incorporate improvements suggested during operation of the instrument this past year. These include:

1. An improved, fast risetime, low jitter trigger,
2. A mount that allows for easier crystal installation and removal,
3. A more easily aligned beam line,
4. Record image with an electronic imaging array (CCD or CID),
5. Slit for imaging the PRS.

These modifications will both improve data quality and shorten the time it takes to be digitized and available for analysis.

The pacing item for spectrometer fabrication is the streak camera itself. The vendor, Kentech Instruments, has quoted a lead time of 4 months for the low magnification camera that we want to purchase. BRA needs to receive a funding increment from DNA (as of October 27th) before the camera can be procured. An advantage to procuring the camera soon is that there is a relatively advantageous monetary exchange rate at this time. The experiments currently planned to start in March at Double EAGLE, will look at large diameter Mg-coated Al wire arrays. The high time resolution of the streak camera will provide interesting details concerning the time evolution of the ion species, electron density, and electron temperature of the x-ray emitting region.

Such measurements could also be done on long implosion type loads of interest to ACE-4. For example, SATURN experiments reported by Rick Spielman indicate that filled cylinder puffs exhibit more stability and higher x-ray yields than hollow shells. This trend is predicted by NRL numerical models. A possible experimental approach to investigate this could use a neon-doped core and a fluorine-doped shell. Streaked spectra could indicate:

1. Stability of the pinch, by how much F from the shell mixes in with the core Ne emission,
2. Plasma conditions, i.e. electron density and temperature, of the pinch from time-resolved line ratios. This measurement approach has been successfully used in inertial confinement fusion (ICF) experiments performed at the NOVA laser at Lawrence Livermore National Laboratory. In that case the core was doped with Ar and the shell with Cl.

The feasibility of recording a continuous, as opposed to framed, x-ray spectra with high temporal resolution has been demonstrated. The streak records indicate a clear difference between the rise and fall times of the PRS that depends on the ionization state of the emitting ion. The spectrometer will be very useful for Mg-coated Al wire array experiments planned for 1996, and also for long implosion time plasma radiation sources, of interest to ACE-4.

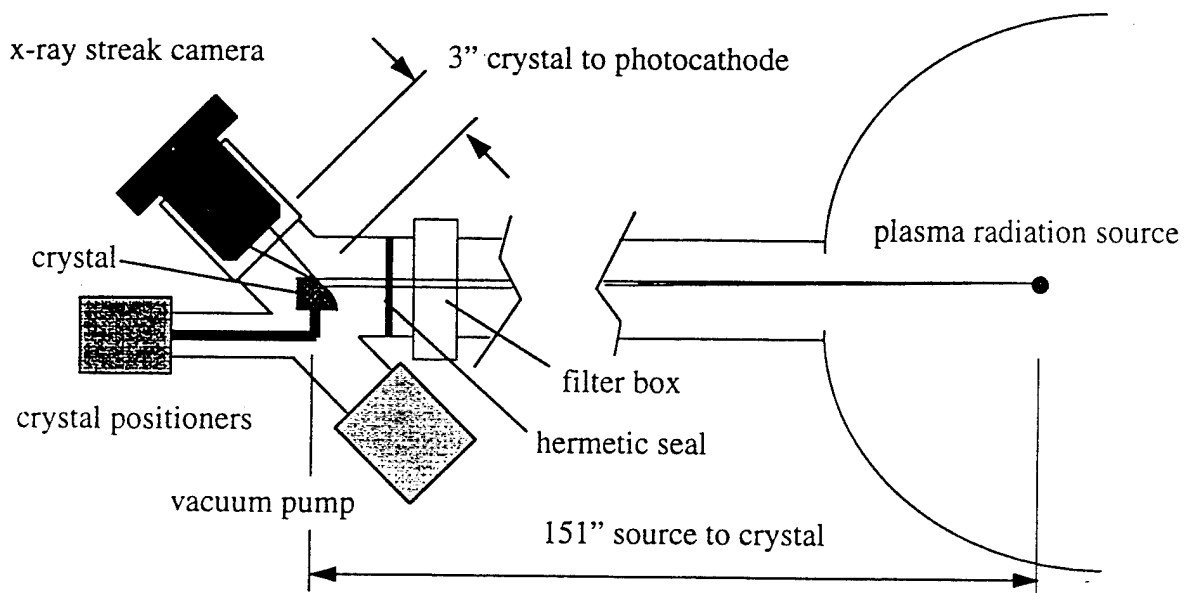


Figure A-1. Geometry of streak camera setup on Double Eagle.

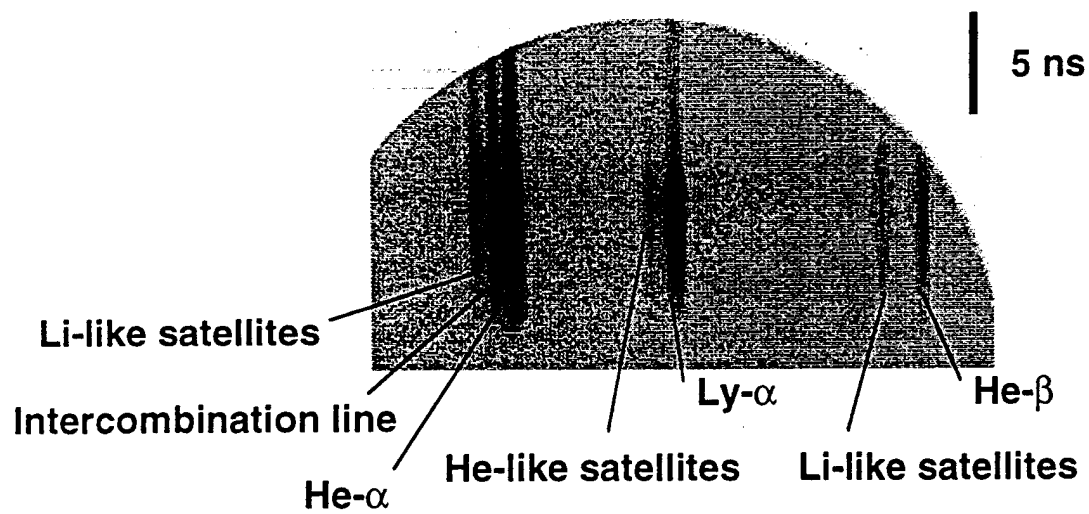


Figure A-2. Streaked spectrum for argon pinch.

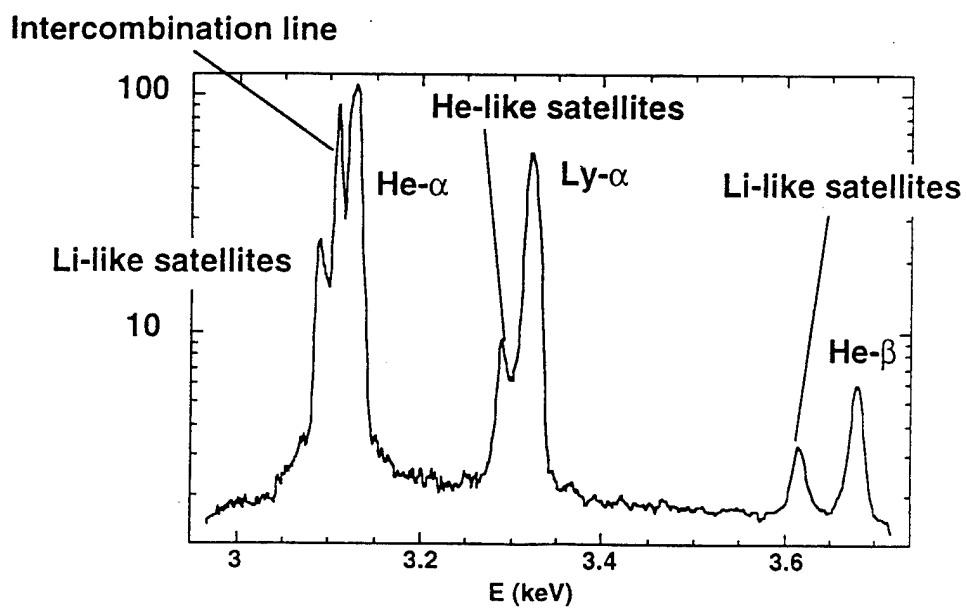


Figure A-3. Densitometer scan of lines at peak emission.

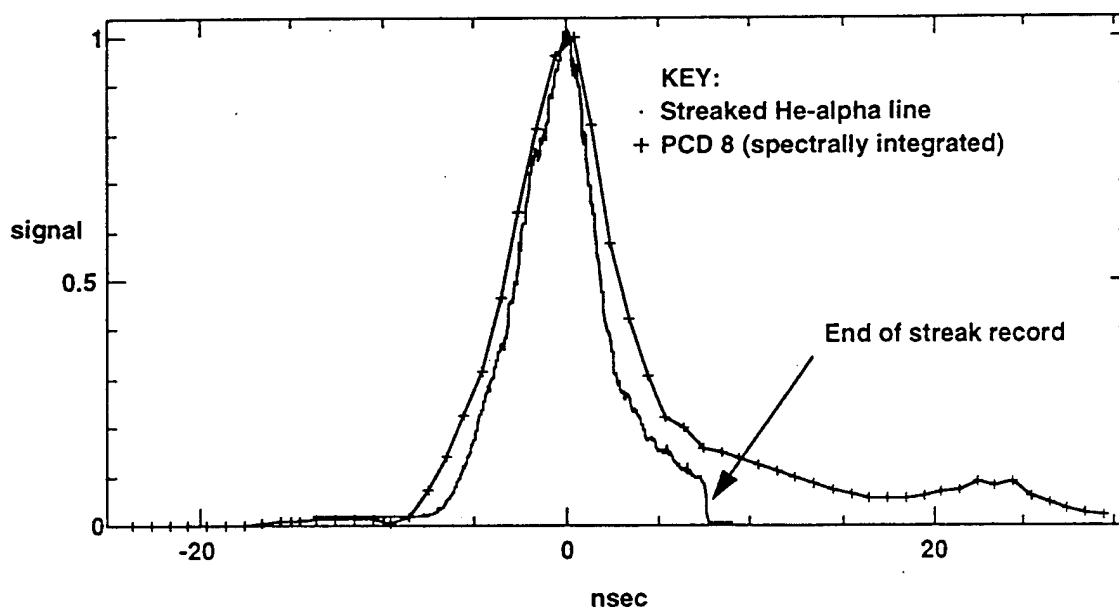


Figure A-4. Spectrally integrated intensity from photodiode (PCD8) compared to streaked  $\text{Ar}_{\text{He}-\alpha}$  line (DE shot 3391).

## DISTRIBUTION LIST

DNA-TR-95-106

### DEPARTMENT OF DEFENSE

DEFENSE INTELLIGENCE AGENCY  
ATTN: DIW-4

DEFENSE NUCLEAR AGENCY  
ATTN: ES JOAN MA PIERRE  
2 CY ATTN: ESA  
ATTN: ESA DR G DAVIS  
ATTN: ESA W SUMMA  
ATTN: ESE  
ATTN: ESE R C WEBB  
ATTN: ESE W J SCOTT  
ATTN: EST K WARE  
ATTN: EST L PRESSLEY  
ATTN: EST R GULLICKSON  
ATTN: EST R SCHNEIDER  
2 CY ATTN: ISST  
ATTN: PMPO  
ATTN: PMPO P HEBERT  
ATTN: WEL  
ATTN: WEP T HOOVER

DEFENSE TECHNICAL INFORMATION CENTER  
2 CY ATTN: DTIC/OCF

FIELD COMMAND DEFENSE NUCLEAR AGENCY  
ATTN: FCTI  
ATTN: FCTT DR BALADI  
ATTN: FCTTR R W SHOUP

### DEPARTMENT OF THE ARMY

ARMY RESEARCH LABORATORIES  
ATTN: TECH LIB  
ATTN: AMSEL-WT-NH G HUTTLIN  
ATTN: AMSEL-WT-NH G A KEHS

U S ARMY COMM R&D COMMAND DEFENSE CMD  
ATTN: CSSD-ES-E1 R CROWSON

U S ARMY CORPS OF ENGINEERS  
ATTN: CERD-M DR LEVERENZ

U S ARMY NUCLEAR & CHEMICAL AGENCY  
ATTN: MONA-NU DR D BASH

U S ARMY TRADOC ANALYSIS CTR  
ATTN: ATRC-WSS-R

USASSDC  
ATTN: CSSD-AT I MERRITT  
ATTN: CSSD-BC-E G POLLOCK  
ATTN: CSSD-WD D BRADSHAW

### DEPARTMENT OF THE NAVY

NAVAL RESEARCH LABORATORY  
ATTN: CODE 6654 DR C D BOND  
ATTN: CODE 6720 J DAVIS  
ATTN: CODE 6770 G COOPERSTEIN

SPACE & NAVAL WARFARE  
ATTN: LCDR J SMITH CODE 32M11  
ATTN: R WOODS CODE 32M12

### DEPARTMENT OF THE AIR FORCE

PHILLIPS LABORATORY  
ATTN: CA AEBY PL/WSSH  
ATTN: D H HILLAND PL/WSSH

SAN ANTONIO AIR LOGISTICS CTR  
ATTN: ALC/SW F CRISTADORO

SPACE SYSTEM DIVISION/XR  
ATTN: SMC/CC  
ATTN: SMC/CNJZ  
ATTN: SMC/CNTZ  
ATTN: SMC/CZEA  
ATTN: SMC/EN  
ATTN: SMC/MBSS  
ATTN: SMC/MGS  
ATTN: SMC/XRX

SSP-27334 TRIDENT  
ATTN: J BURTLE  
ATTN: K TOBIN

USAF/AEDC/DOT  
ATTN: CAPT F FAIRCHILD DOT

### DEPARTMENT OF ENERGY

LAWRENCE LIVERMORE NATIONAL LAB  
ATTN: J NUCKOLLS  
ATTN: G SIMONSON  
ATTN: M TOBIN

LOS ALAMOS NATIONAL LABORATORY  
ATTN: C EKDAHL  
ATTN: J BROWNELL

SANDIA NATIONAL LABORATORIES  
ATTN: L M CHOATE  
ATTN: M HEDEMANN  
ATTN: M K MATZEN  
ATTN: D COOK  
ATTN: R E PEPPING  
ATTN: TECH LIB 3141  
ATTN: W BALLARD  
ATTN: W BEEZHOLD

U.S. DEPARTMENT OF ENERGY  
OFFICE OF MILITARY APPLICATIONS  
ATTN: C B HILLAND  
ATTN: R DEWITT  
ATTN: R GUNDERSON

### OTHER GOVERNMENT

CENTRAL INTELLIGENCE AGENCY  
ATTN: OSWR J PINA

### DEPARTMENT OF DEFENSE CONTRACTORS

ADVANCED RESEARCH & APPLICATIONS CORP  
ATTN: R ARMISTEAD

AEROSPACE CORP  
ATTN: LIBRARY ACQUISITION  
ATTN: T PARK

**DNA-TR-95-106 (DL CONTINUED)**

ALME & ASSOCIATES  
ATTN: JOHN F DAVIS  
ATTN: S SEILER

APTEK, INC  
ATTN: T MEAGHER

BDM FEDERAL INC  
ATTN: W BETOWT  
ATTN: W LARRY JOHNSON

BERKELEY RSCH ASSOCIATES, INC  
2 CY ATTN: N PEREIRA

CALSPAN CORP/AEDC  
ATTN: L S CHRISTENSEN  
ATTN: V KENYON

DEFENSE GROUP, INC  
ATTN: ROBERT POLL

HUGHES AIRCRAFT COMPANY  
ATTN: SCG-S41/B36G  
ATTN: 5CG-S41/B366

HY-TECH RESEARCH CORP  
2 CY ATTN: E J YADLOWSKY

JAYCOR  
ATTN: J R MILLARD  
ATTN: T FLANAGAN

JAYCOR  
ATTN: CYRUS P KNOWLES  
ATTN: R SULLIVAN

JAYCOR  
ATTN: C ROGERS  
ATTN: S ROGERS

KAMAN SCIENCES CORP  
ATTN: D CALDWELL  
ATTN: D JANSEN

KAMAN SCIENCES CORP  
ATTN: CLAUDE FORE  
ATTN: E DRISCOLL

KAMAN SCIENCES CORPORATION  
ATTN: DASIAK

KTECH CORP  
ATTN: FRANK DAVIES

LOGICON R & D ASSOCIATES  
ATTN: I VITKOVITSKY

LOGICON R & D ASSOCIATES  
ATTN: ROGER LEWIS

MAXWELL LABORATORIES INC  
ATTN: D PARKS  
ATTN: DR G GURTMAN  
ATTN: J M WILKENFELD  
ATTN: WAISMAN

MAXWELL LABS  
ATTN: JOHN THOMSON  
ATTN: PHIL COLEMAN  
ATTN: WILLIAM H RIX

MISSION RESEARCH CORP  
ATTN: J R HENLEY

PHYSICAL SCIENCES, INC  
ATTN: JOHN F DAVIS  
ATTN: S SEILER

PHYSICS INTERNATIONAL CO  
ATTN: B FAILOR  
ATTN: C STALLINGS  
ATTN: DAVID LEPELL  
ATTN: J RIORDAN  
ATTN: P SINCERNY  
ATTN: S L WONG

PULSE SCIENCES, INC  
ATTN: I D SMITH  
ATTN: P W SPENCE

SCIENCE APPLICATIONS INTL CORP  
ATTN: W CHADSEY

THE AEROPSACE CORP  
ATTN: M HOPKINS

W J SCHAFER ASSOCIATES, INC  
ATTN: E ALCARAZ